The Thesis Committee for Christopher Martin Crittenden
Certifies that this is the approved version of the following thesis:

Tandem Mass Spectrometry Approaches to Characterizing Challenging Biomolecules: Stapled and Cyclic Peptides and Variants of Lipid A from Gram-negative Bacteria

APPROVED BY
SUPERVISING COMMITTEE:

Supervisor:

Jennifer S. Brodbelt

Charles Buddie Mullins

Tandem Mass Spectrometry Approaches to Characterizing Challenging Biomolecules: Stapled and Cyclic Peptides and Variants of Lipid A from Gram-negative Bacteria

by

Christopher Martin Crittenden, B.S.Ch.

Thesis

Presented to the Faculty of the Graduate School of

The University of Texas at Austin

in Partial Fulfillment

of the Requirements

for the Degree of

Master of Arts

The University of Texas at Austin

August 2016

Acknowledgements

The guidance and mentorship provided by the thesis supervisor, Jennifer Brodbelt, throughout the duration of this work is greatly acknowledged and appreciated. Funding for this research was provided by the NSF and Welch Foundation. I also greatly acknowledge the support and confidence given to me by my wife, Shastina L. Oglesbee, and my daughter, Evelynn I. Crittenden.

Abstract

Tandem Mass Spectrometry Approaches to Characterizing Challenging Biomolecules: Stapled and Cyclic Peptides and Variants of Lipid A from Gram-negative Bacteria

Christopher Martin Crittenden, M.A.

The University of Texas at Austin, 2016

Supervisor: Jennifer S. Brodbelt

Mass spectrometry has emerged as a leading tool in the field of chemistry as an analytical method for the characterization of small molecules, proteins, and other complex biomolecules. Specifically, cyclic and stapled peptides have become an intriguing class of biomolecules in drug research afforded to them because of their biological stability and resistance to proteolytic digestions. However, challenges are presented in regards to the characterization of these molecules as traditional methods are ineffective in determining a ring-opening site on the peptidic backbone. Additionally, lipid A, the hydrophobic domain of lipopolysaccharide (LPS), consists of a diglucosamine backbone and is responsible for fastening LPS to a membrane surface. Lipid A becomes a biologically relevant molecule to study as its function within LPS is directly related to the infectious and toxic properties of gram-negative bacteria, but the molecule is structurally complex and offers many challenges in terms of traditional mass spectrometry characterization. Presented in the thesis are methods to further comprehend

structural motifs related to the aforementioned biomolecules. The “ornithine effect”, which describes the conversion of an arginine residue to an ornithine residue via reaction with hydrazine and subsequent preferential cyclization via nucleophilic attack of the ornithine side-chain to the neighboring carbonyl group, inducing heterolytic cleavage of the adjacent amide bond under gentle activation, is used to preferentially open cyclic and stapled rings to linearize these challenging biomolecules. Ramped collisional and photon based activation (in terms of energy and laser pulses) of lipid A molecules that contain differences in acyl-chain length and connectivity reveal general trends about the lability of certain bonds on the lipid A molecules themselves and paints a picture of the overall fragmentation trends associated with variations in lipid A structural motifs.

Table of Contents

List of Tables

List of Figures

List of Schemes

Chapter One: Exploitation of the Ornithine Effect Enhances Characterization of Stapled and Cyclic Peptides[1]

OUTLINE 1.1

A method to facilitate the characterization of stapled or cyclic peptides is reported via an arginine-selective derivatization strategy coupled with MS/MS analysis. Arginine residues are converted to ornithine residues through a deguanidination reaction that installs a highly selectively cleavable site in peptides. Upon activation by CID or UVPD, the ornithine residue cyclizes to promote cleavage of the adjacent amide bond. This Arg-specific process offers a unique strategy for site-selective ring opening of stapled and cyclic peptides. Upon activation of each derivatized peptide, site-specific backbone cleavage at the ornithine residue results in two complementary products: the lactam ring-containing portion of the peptide and the aminecontaining portion. The deguanidination process not only provides a specific marker site that initiates fragmentation of the peptide but also offers a means to unlock the staple and differentiate isobaric stapled peptides.

INTRODUCTION 1.2

Cyclic, stapled, and branched peptides constitute a unique and growing class of biomolecules with promise as therapeutics because of their biostability and resistance to proteolytic digestion in physiological environments [1–7]. In the context of therapeutics, peptide-based drug candidates display both advantages and disadvantages in comparison to their small molecule counterparts. Peptides, while frequently less toxic than small

[1] Crittenden, C.M., Parker, W.R., Jenner, Z.B., Bruns, K.A., Akin, L.D., McGee, W.M., Ciccimaro, E., Brodbelt, J.S.: Exploitation of the Ornithine Effect Enhances Characterization of Stapled and Cyclic Peptides. J. Am. Soc. Mass Spectrom. (2016) 27:856-863. Research funding provided by the NSF and the Welch Foundation. CMC's contributions: experimental design, execution, and analysis.

molecules when administered intravenously and exhibiting higher selectivity for specific biological functions, do not traverse cell membranes with the ease that small molecules do and are prone to proteolytic degradation [8, 9]. However, peptides that are protected from degradation via cyclization or stapling have been shown to exhibit high potency and low toxicity, resulting in more promising candidates for drug administration than their linear counterparts [3–7]. A myriad of nonlinear peptides are found naturally in plants, fungi, and bacteria as well as synthetic ones produced in the laboratory [10–18]. Valinomycin, for example, is a cyclic dodecadepsipeptide produced by *Streptomyces fulvissimus* with potent antibacterial properties while also acting as a potassium-selective ionophore [19, 20]. Enzyme inhibition is another pharmaceutical application that is associated with cyclic peptides, as shown by two examples of the Bowman-Birk class of protease inhibitors, Sunflower trypsin inhibitor-1 (SFTI-1) and *Momordica cochinchinensis* trypsin inhibitor-II (MCoTI-II) [21].

From an analytical standpoint, structural characterization of cyclic or stapled peptides is significantly more challenging than elucidation of linear peptides. The success of tandem mass spectrometry for sequencing peptides is based on production of predictable N-terminus and C-terminus fragment ions via cleavage of the peptide backbone. Cyclic peptides require cleavage of two backbone bonds to generate fragment ions, and the lack of natural N-terminal and C-terminal positions confounds an orderly mapping of the sequence of residues. Stapled peptides suffer from a similar pitfall in the region of the peptide containing the stapled (cyclized) portion and also typically contain hydrocarbon (non-peptide-like) linkers that constitute the staple. Several mass

spectrometric techniques, including collision induced dissociation (CID) [20–25], MS^n methods [23, 25–27], electron capture dissociation (ECD) [28], and complexation strategies [29, 30], have emerged as the most valuable tools to assist in the characterization of the sequences of non-linear peptides.

In addition to the use of MS^n methods to facilitate the characterization of cyclic and stapled peptides, another synergistic strategy evolves from site-selective fragmentation processes that may be used to "anchor" a particular location in a molecule based on a site-specific cleavage. Once an anchor point is established, all other fragmentation pathways and the resulting product ions can be referenced to the anchor point. Highly selective or preferential bond-specific cleavages remain relatively rare occurrences upon activation of peptides and proteins. As one example, the proline effect is one of the few well-established site-specific cleavage upon activation, occurring N-terminal to proline residues due to the increased basicity of the N-alkylated amide bond as well as the increased steric hindrance about the residue [31, 32]. The proline directed cleavage creates a readily recognized fragment ion in the MS/MS spectra of peptides. Along these lines, there has been renewed interest in the development of peptide derivatization strategies to install tags with labile bonds or ones with selectively cleavable groups in order to promote bond-selective cleavages [33–39]. Recently, the "ornithine effect" has been reported as a site-specific cleavage occurring C-terminal to ornithine residues [40, 41]. Upon collisional activation of an ornithine-containing peptide, the amine of the ornithine residue cyclizes via nucleophilic attack at the adjacent carbonyl group, resulting in a characteristic and preferential cleavage C-terminal to the carbonyl

group. This phenomenon has been observed before, as lysine and many of its homologues have exhibited similar characteristics as a nucleophile previously [42–45].

The present study explores the utility of the ornithine effect to enhance the characterization of cyclic and stapled peptides. By exploiting the predictability of the ornithine effect, unique ions are generated that allow the differentiation of isomers. Both collision-based and photon-based activation methods are used to characterize the modified and unmodified peptides. The fragment ions were assigned using an in-house algorithm designed to systematically generate a list of every possible combination of bond cleavages (including cross-ring cleavages) and the associated masses of the fragments.

EXPERIMENTAL 1.3

Materials and Reagents

HPLC grade water and methanol used for sample preparation and dilution were purchased from EMD Millipore (Billerica, MA, USA) and formic acid was purchased from Fisher Scientific (Fairlawn, NJ, USA). Sunflower trypsin inhibitor-1 (SFTI- 1) was provided by Bristol-Myers Squibb (Princeton, NJ, USA). Dithiothreitol (DTT) and iodoacetamide (IAM) used for reduction and alkylation of disulfide bonds were purchased from Sigma Aldrich (St. Louis, MO, USA). Proteomics-grade trypsin was obtained from Promega (Madison, WI, USA).

Synthesis and Purification of Stapled Peptides

Stapled peptides were produced by BioSynthesis (Lewisville, TX, USA) using Fmoc solid phase peptide synthesis. Peptides were stapled by ring-closing metathesis

using Grubbs' First Generation Catalyst, and purified by preparative C18 reversedphase HPLC. The purity of the peptides was confirmed as >95% by analytical HPLC and by MALDI-TOF MS.

Sample Preparation

Unmodified samples were diluted to 5 uM with an equal mixture of methanol and water with 1% formic acid prior to direct infusion ESI. Stapled peptides and SFTI-1 were mixed with excess hydrazine hydrate for 4 h at 55 °C in water to promote the conversion of arginine to ornithine. The reaction mixture was dried under vacuum (Thermo Savant DNA 120 Speedvac Concentrator, San Jose, CA, USA) to remove organics and diluted to 5 uM with an equal mixture of methanol and water with 1% formic acid prior to direct infusion ESI. After the incubation of SFTI-1 with hydrazine hydrate, the intramolecular disulfide bond was reduced with dithiothreitol (100 mM in water) for 45 min at 55 °C and alkylated with iodoacetamide (100 mM in water) for 45 min protected from light at room temperature.

Mass Spectrometry and Photodissociation

All MS experiments were performed on a Thermo Scientific Orbitrap Elite mass spectrometer (San Jose, CA, USA) custom fit with an unfocused, non-collimated Coherent ExciStar 193 nm excimer laser (Santa Clara, CA, USA) to perform ultraviolet photodissociation, as previously described [46, 47]. Peptides, both modified and unmodified, were analyzed by direct infusion electrospray ionization with a spray voltage of 4 kV and a capillary temperature of 275 °C. For all CID experiments, the normalized collision energy (NCE) was varied to reduce the precursor to approximately 10%– 15%

relative abundance during an activation period of 10 ms (this is sufficient to provide rich fragmentation without excessive ejection of the precursor ion during resonance excitation). For all UVPD experiments, a laser power of 1.5–2.5 mJ/pulse and one to three 5-ns pulses were used. The resulting MS/MS spectra were interpreted manually as well as by using a custom fragment ion prediction algorithm that was developed in-house.

Development of a Custom Algorithm for Assignment of Fragment Ions

Several algorithms have recently been developed to assist with the characterization of cyclic peptides. Two of the most recent algorithms are CYCLONE and CycloBranch, which were developed to characterize cyclic peptides via a de novo strategy [48, 49]. An in-house algorithm was developed in C# to assign fragment ions of cyclic peptides based on interpretation of 193 nm UVPD mass spectra. Unlike CYCLONE and CycloBranch, this algorithm utilizes a naïve approach that calculates all potential fragment ions which may arise from the cleavage of any bond in the peptide's structure and cross-ring cleavages based on candidate structures. Moreover, the custom algorithm accepts any type of candidate structure, including stapled peptides containing unnatural amino acids, unlike other available algorithms. The structures of the candidate peptides were generated in ChemDraw Perkin Elmer (Waltham, MA, USA). The structures were assigned atom numbers and implicit hydrogens were selected to be hidden. The final structure was saved as a cdxml file. The XML from the cdxml files were then parsed by the algorithm and converted into an undirected graph (abstract data structure). A naïve approach was employed in which fragments were calculated through the systematic removal of each edge in the graph from the candidate molecule's structure.

Additionally, with a ring size specified, fragments resulting from cross ring cleavages could also be calculated (resulting from the cleavage of two bonds). These calculated fragment ions were saved in a SQLite database [50], which could be exported into an Excel file. The ions in the MS/MS spectra were then manually compared with the theoretically calculated masses.

RESULTS AND DISCUSSION 1.4

Conversion of arginine to ornithine by deguanidination in the presence of hydrazine causes a mass shift of 42 Da, as shown in **Scheme 1.1**. Subsequent activation of an ornithine-containing peptide may result in cyclization via nucleophilic attack of the side-chain amine of the ornithine residue on a neighboring carbonyl carbon, causing a heterolytic cleavage of the adjacent amide bond. This process is referred to as the "ornithine effect," and, in short, is based on a decrease in proton affinity in the gas phase when an arginine residue is converted to an ornithine residue (see reference [40] for a complete explanation of the ornithine effect and see reference [42], which reports the gas-phase proton affinity of ornithine). This site-specific cleavage affords a facile, predictable fragmentation pathway for arginine-containing peptides and offers a convenient way to convert cyclic peptides into acyclic ones. In this study, both CID and UVPD are implemented to induce the ornithine effect as a means to simplify the characterization of stapled and cyclic peptides.

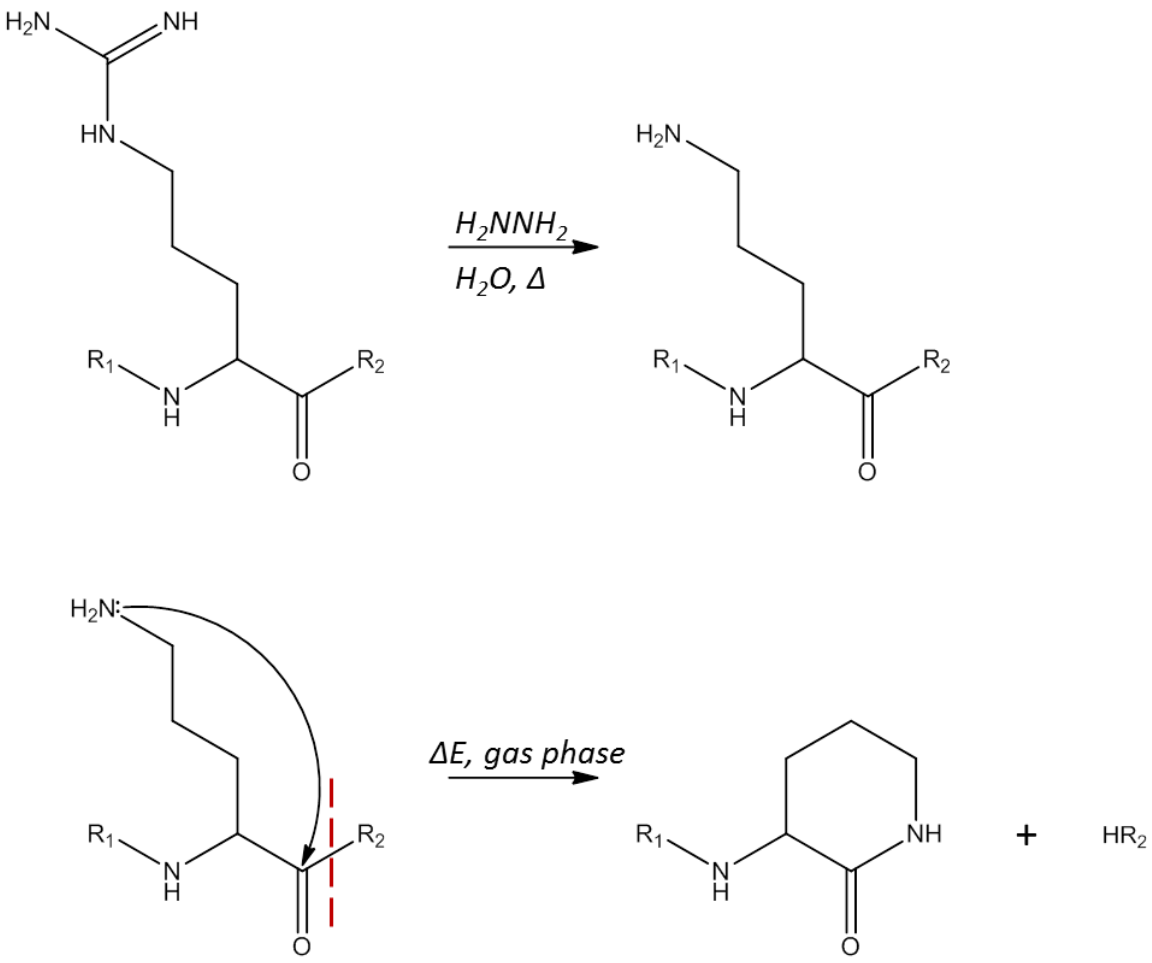

Scheme 1.1. Conversion of an arginine residue into an ornithine residue results in a mass shift of 42 Da and proceeds in the presence of hydrazine. Upon gas phase activation, the ornithine residue cyclizes via nucleophilic attack and the adjacent amide bond is heterolytically cleaved. This figure is adapted from Ref. 40.

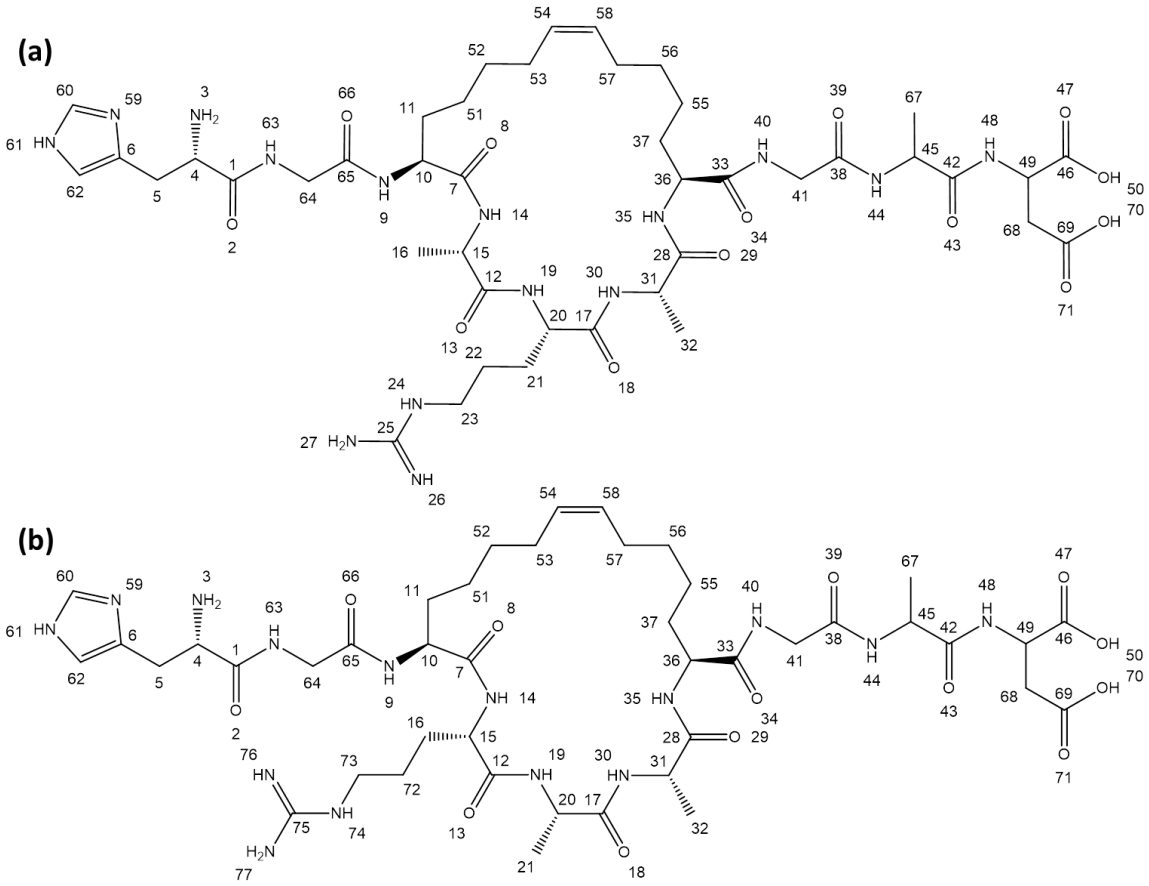

Figure 1.1. Structure of the stapled peptide, (a) [H_2N]-HG-X-ARA-X-GAD-[CO_2H] (Mr = 1004.12 Da) and (b) [H_2N]-HG-X-RAA-X-GAD-[CO_2H] (Mr = 1004.12 Da). The stapled pentenyl alanines are located between atom numbers 10 and 36. The "X" represents pentenyl alanine residues that have been stapled together through ruthenium catalyzed ring-closure metathesis.

When analyzing the MS/MS spectra of stapled and cyclic peptides, there is an inherent challenge in nomenclature associated with the fragment ions due to the presence of multiple branches or the lack of any terminal positions. In this study, an in-house algorithm was developed to assist in the identification and assignment of the resulting fragment ions. For the stapled and cyclic peptides, a fragment ion involving the cyclic portion can only be produced via cleavages of two bonds (one in the cyclic region and

one in the linear segment, typically creating an internal ion) or via a cross-ring cleavage. A single bond cleavage between atom numbers 1 and 2 is annotated as "[atom number 1 | atom number 2]" and the cleavage of two bonds between atom numbers 1 and 2 and atom numbers 3 and 4 simultaneously is annotated as "[atom number 1 | atom number 2 || atom number 3 | atom number 4]". If multiple cleavages lead to the same *m/z* ratio, all possible fragments are listed.

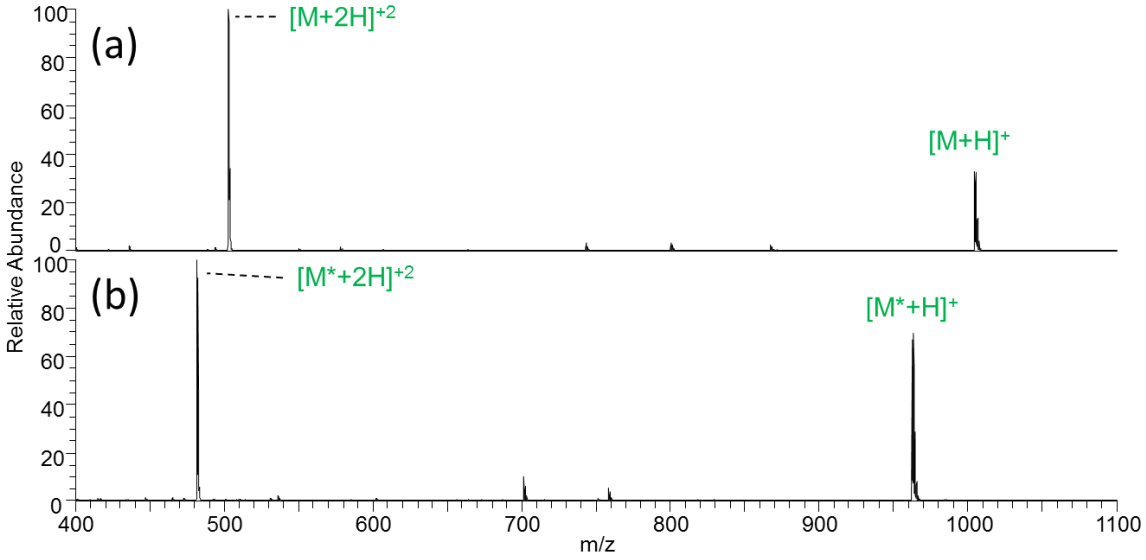

Figure 1.2. ESI mass spectrum of (a) unmodified stapled peptide [H_2N]-HG-X-RAA-X-GAD-[CO_2H] and (b) modified stapled peptide [H_2N]-HG-X-OAA-X-GAD-[CO_2H]. An asterisk (*) represents presence of the modification from arginine to ornithine. The "X" represents pentenyl alanine residues that have been stapled together through ruthenium catalyzed ring-closure metathesis.

Two variants of a stapled peptide with sequences [H_2N]- HG-X-ARA-X-GAD-[CO_2H] and [H_2N]-HG-X-RAA-XGAD-[CO_2H] (**Figure 1.1**) were characterized. The "X" represents pentenyl alanine residues that have been stapled together through

ruthenium-catalyzed ring-closure metathesis.The ESI mass spectra of one of the unmodified and ornithine-modified stapled peptides (**Figure 1.2**) show that the conversion of the stapled peptide to the ornithine-containing analogue was an efficient reaction. As demonstrated in **Figure 1.3**, the CID mass spectra of the two unmodified stapled peptides are nearly identical, resulting in no fragment ions that are unique to either of the two isomeric peptides (fragmentation maps for the unmodified stapled peptides are shown in **Figure 1.4**).

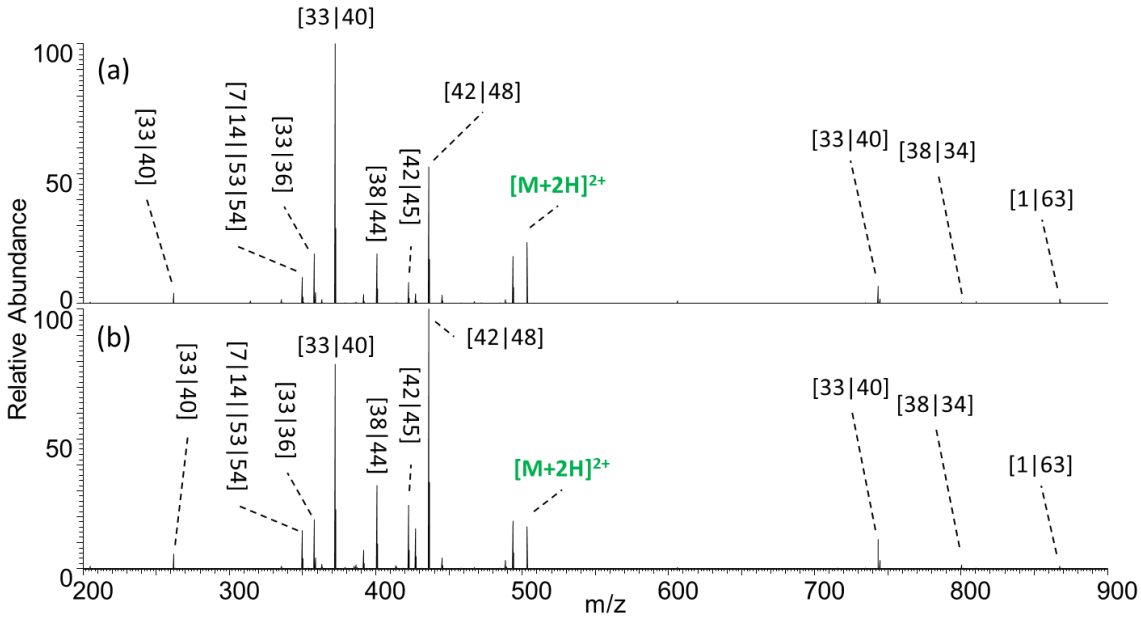

Figure 1.3. CID mass spectra (240K resolution) of unmodified stapled peptides. (a) $[H_2N]$-HG-X-ARA-X-GAD-$[CO_2H]$. (b) $[H_2N]$-HG-X-RAA-X-GAD-$[CO_2H]$. The "X" represents pentenyl alanine residues that have been stapled together through ruthenium catalyzed ring-closure metathesis.

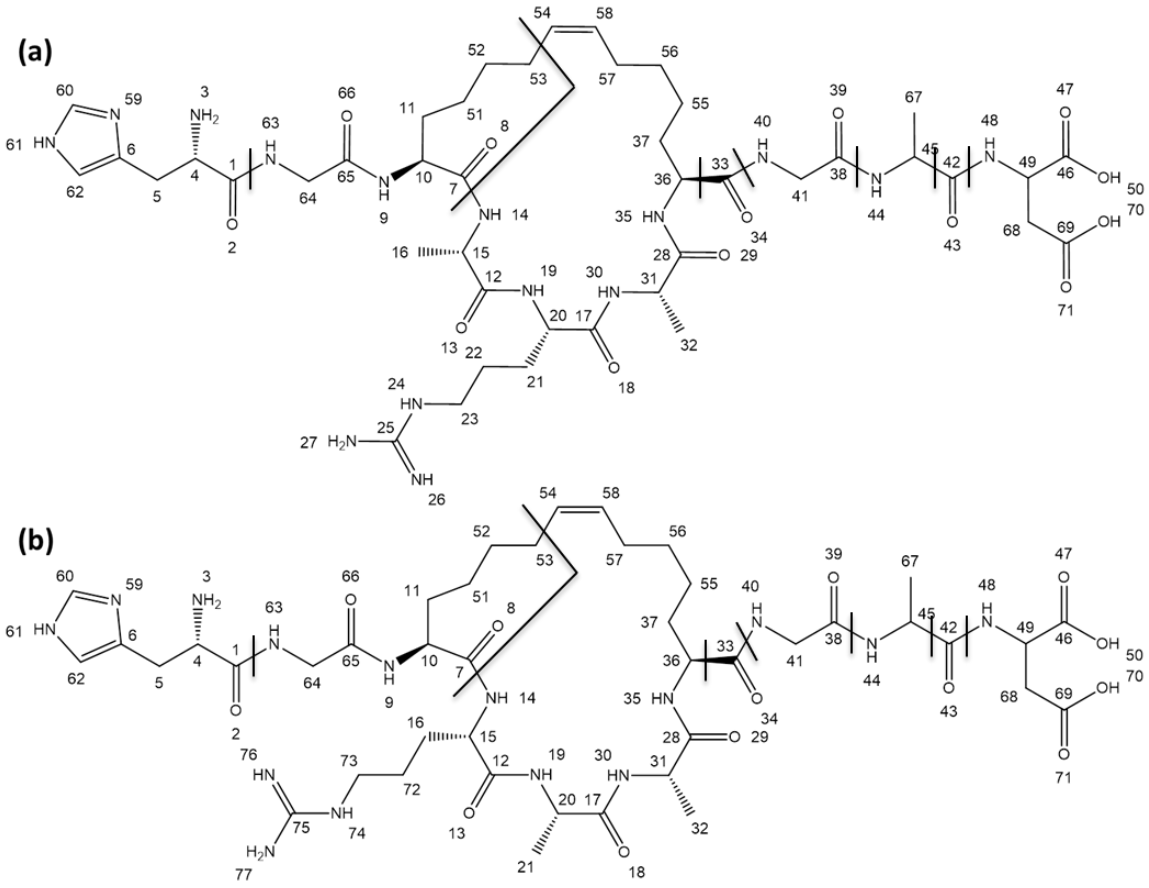

Figure 1.4. Fragmentation maps obtained using CID (240K resolution) of unmodified stapled peptides. (a) $[H_2N]$-HG-X-ARA-X-GAD-$[CO_2H]$. (b) $[H_2N]$-HG-X-RAA-X-GAD-$[CO_2H]$. The "X" represents pentenyl alanine residues that have been stapled together through ruthenium catalyzed ring-closure metathesis. Unique fragment ions detected for the ornithine-containing peptides are indicated in red.

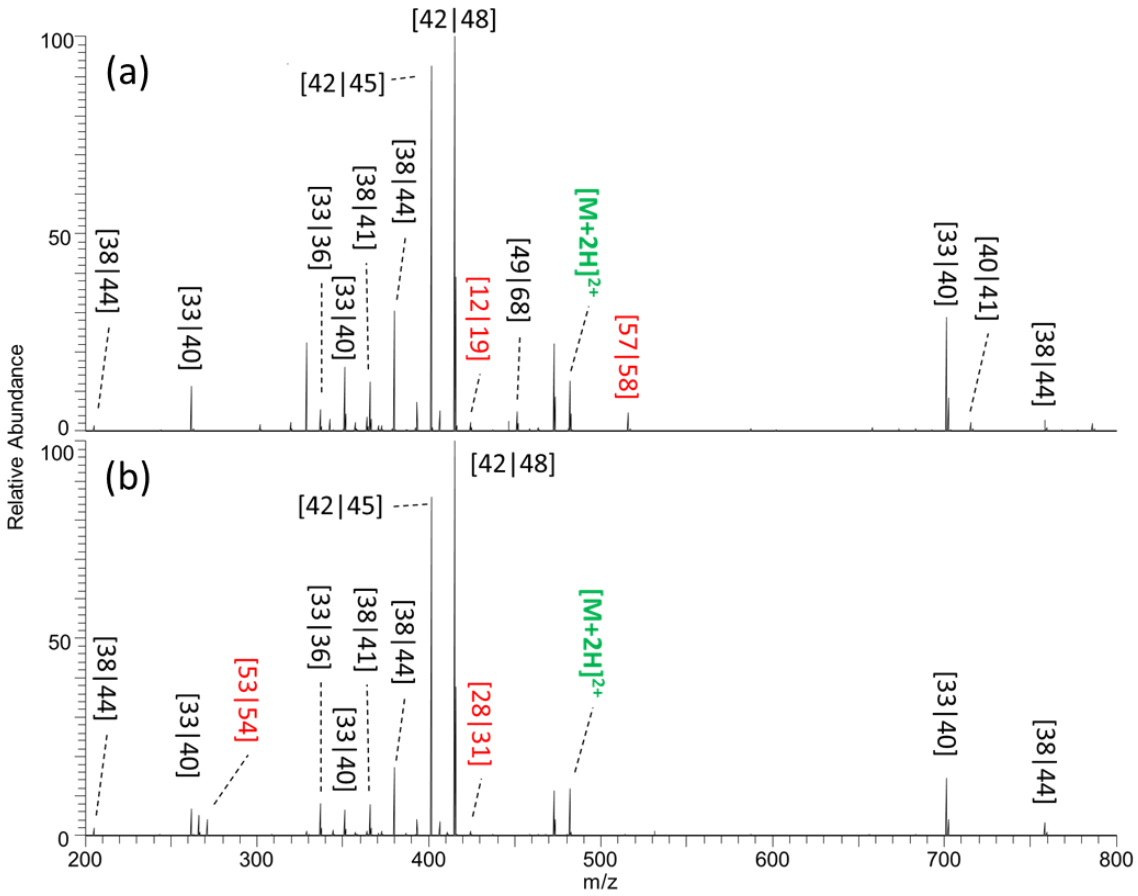

Figure 1.5. CID mass spectra (240K resolution) of ornithine-containing stapled peptides. (a) [H_2N]-HG-X-AOA-X-GAD-[CO_2H]. (b) [H_2N]-HG-X-OAA-X-GAD-[CO_2H]. The "X" represents pentenyl alanine residues that have been stapled together through ruthenium catalyzed ring-closure metathesis. Red labels designate the unique fragment ions between the isobaric stapled peptides (regions around the fragments identified as [57|58] and [53|54] have been magnified 5x for clarity). See expanded regions of the spectra in **Figure 1.4** and **Figure 1.6** showing the differences in fragment ions between the two ornithine-containing stapled peptides.

However, after conversion of the Arg residues to ornithine groups, unique fragments are identified for each (**Figure 1.5**). Cleavages between atoms numbered 57 and 58 (annotated as [57|58]) and 12 and 19 ([12|19]) for [H_2N]-HG-X-AOA-XGAD-

[CO_2H] and cleavages between atoms numbered 53 and 54 ([53|54]) and atoms numbered 28 and 31 ([28|31]) for [H_2N]-HG-X-OAA-X-GAD-[CO_2H] are observed. Expanded regions of these key parts of the spectra are shown in **Figure 1.6** and **Figure 1.7**. Fragmentation maps for each of the two modified stapled peptides are shown in **Figure 1.8**. The two unmodified isomeric peptides have no unique fragment ions in the MS/MS spectra, making the identification of location of the arginine residue within the stapled region impossible. However, as shown in **Figure 1.8a** and **Figure 1.8b**, there is clear indication that the ring opening and lactam formation arising from the ornithine effect lead to generation of unique product ions upon MS/MS.

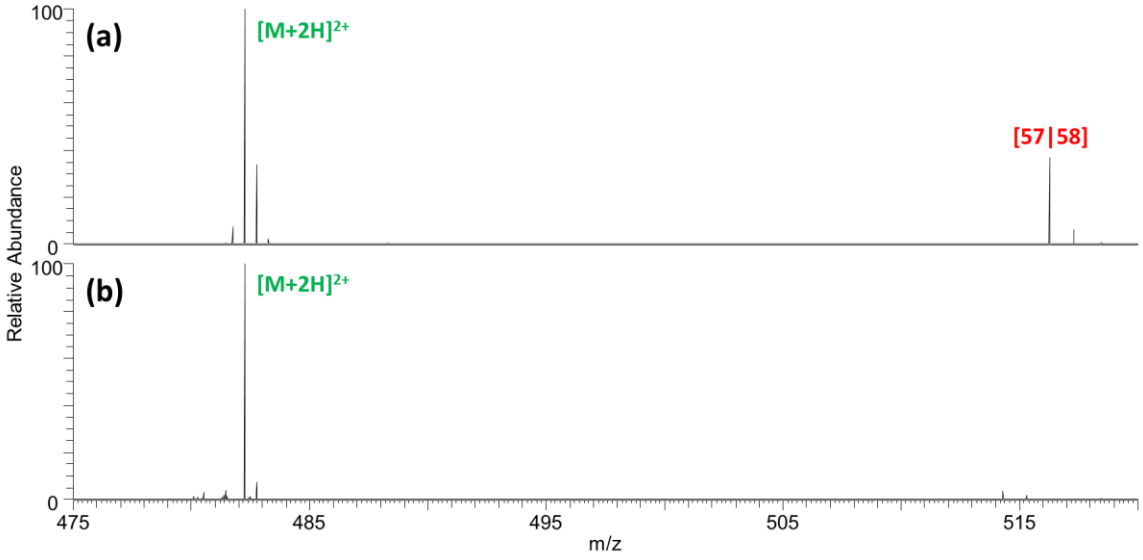

Figure 1.6. Expanded regions of CID mass spectra between m/z 475 and 520 of (a) [H_2N]-HG-X-AOA-X-GAD-[CO_2H] and (b) [H_2N]-HG-X-OAA-X-GAD-[CO_2H] highlighting some of the major differences between the spectra of the ornithine-modified isomers. The "X" represents pentenyl alanine residues that are stapled together through ruthenium catalyzed ring-closure metathesis.

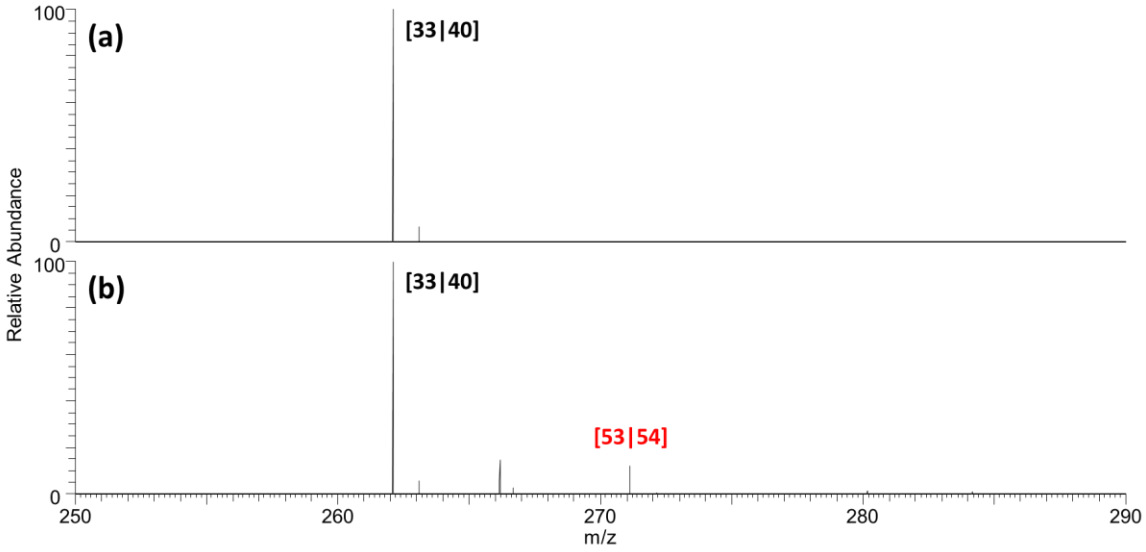

Figure 1.7. Expanded regions of CID mass spectra between 250 m/z and 290 m/z of (a) [H_2N]-HG-X-AOA-X-GAD-[CO_2H] and (b) [H_2N]-HG-X-OAA-X-GAD-[CO_2H] highlighting some of the major differences between the two spectra. The "X" represents pentenyl alanine residues that have been stapled together through ruthenium catalyzed ring-closure metathesis.

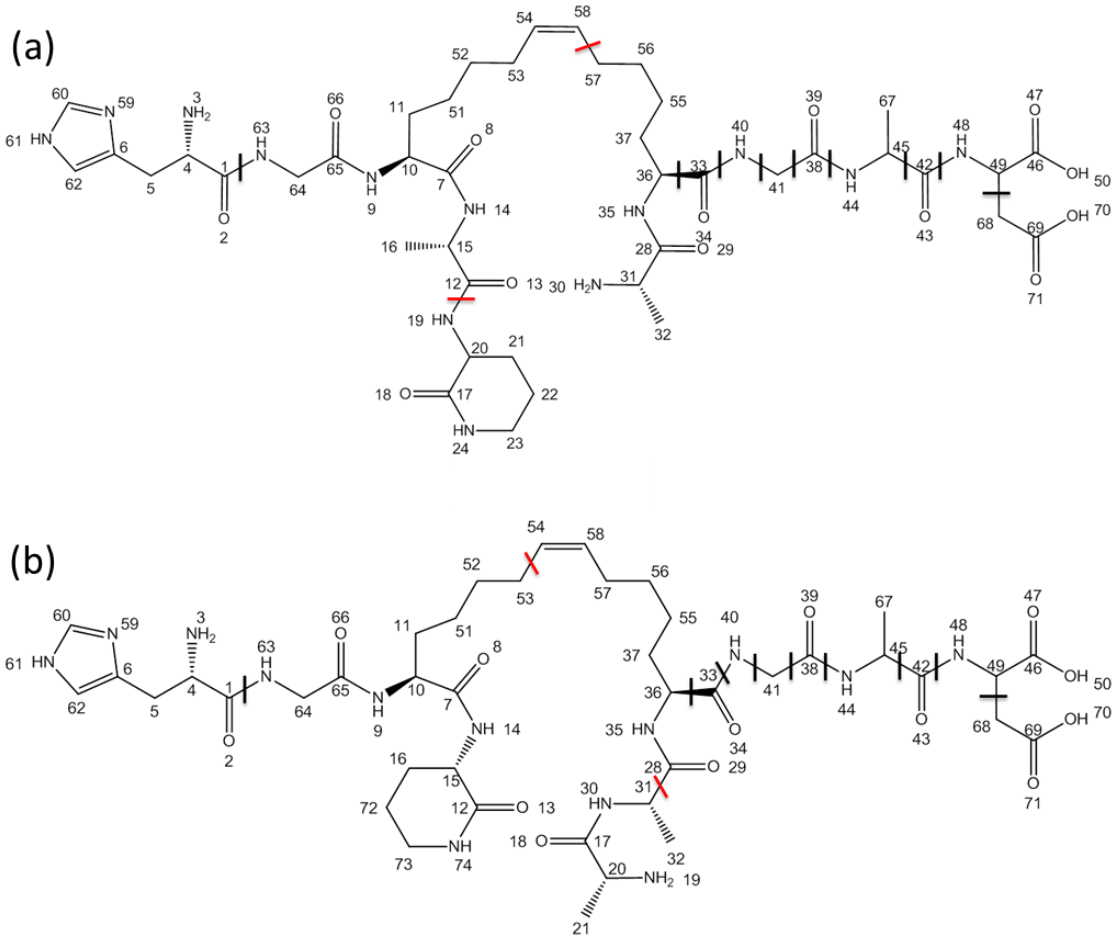

Figure 1.8. Fragmentation maps obtained using CID (240K resolution) of ornithine-containing stapled peptides. (a) [H_2N]-HG-X-AOA-X-GAD-[CO_2H]. (b) [H_2N]-HG-X-OAA-X-GAD-[CO_2H]. The "X" represents pentenyl alanine residues that have been stapled together through ruthenium catalyzed ring-closure metathesis. Unique fragment ions detected for the ornithine-containing peptides are indicated in red.

The unique ions of particular interest evolve from cleavages [12|19] and [57|58] for [H_2N]-HG-X-AOA-XGAD-[CO_2H], and [28|31] and [53|54] for [H_2N]-HG-XOAA-X-GAD-[CO_2H]. In addition to the CID spectra detailed here, the UVPD mass spectra and associated fragmentation maps are shown in **Figure 1.9** and **Figure 1.10**. A few additional unique fragment ions are produced by UVPD of the ornithine-modified peptides relative to the unmodified peptides. As another approach, stapled peptides containing proteolytically recognized residues, such as Arg or Lys, can be subjected to proteolysis to cleave the cyclic stapled segment. The products generated upon tryptic digestion of the two stapled peptides are shown in **Figure 1.11**, **Figure 1.12**, and **Figure 1.13**. Tryptic digestion can result in more complex mixtures if multiple arginine and lysine residues are present.

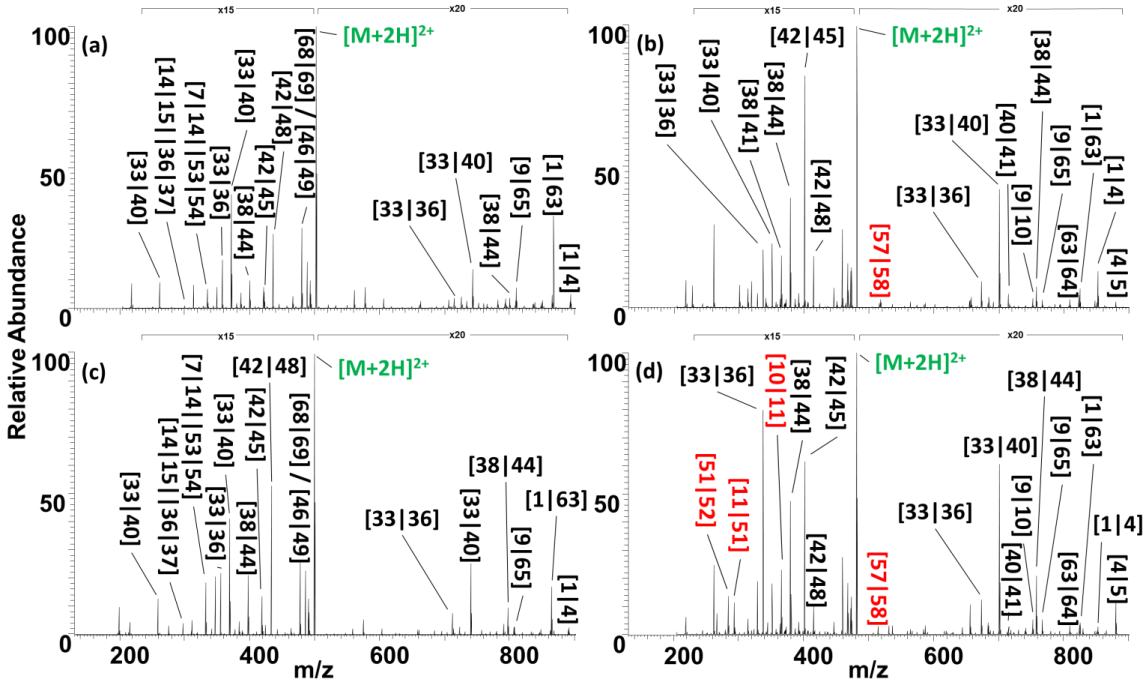

Figure 1.9. UVPD mass spectra (2.5 mJ, 3 pulses, 240K resolution) of arginine- and ornithine-containing stapled peptides. (a) [H_2N]-HG-X-ARA-X-GAD-[CO_2H]. (b) [H_2N]-HG-X-AOA-X-GAD-[CO_2H]. (c) [H_2N]-HG-X-RAA-X-GAD-[CO_2H]. (d) [H_2N]-HG-X-OAA-X-GAD-[CO_2H]. The "X" represents pentenyl alanine residues that have been stapled together through ruthenium catalyzed ring-closure metathesis. Red labels designate the unique fragment ions between the isobaric stapled peptides.

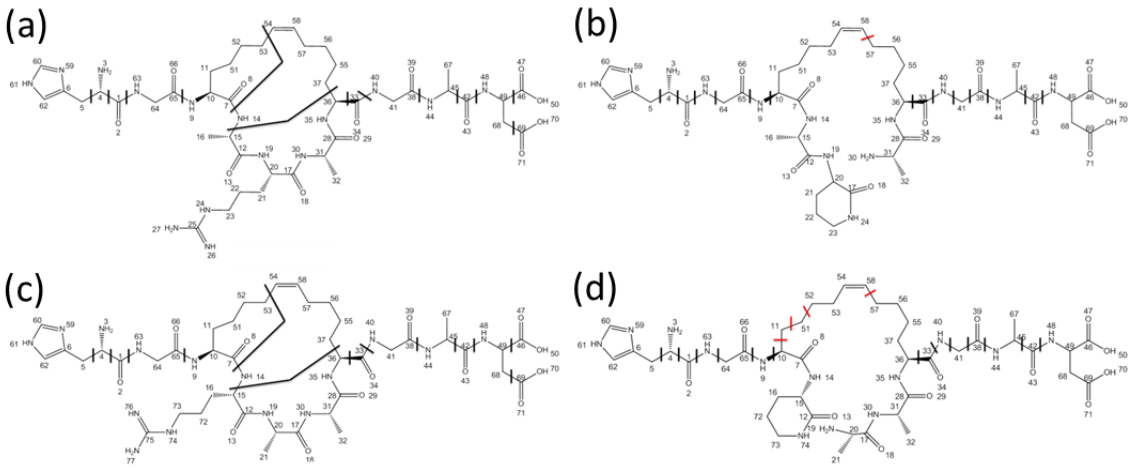

Figure 1.10. Fragmentation maps obtained using UVPD (2.5 mJ, 3 pulses, 240K resolution) of arginine- and ornithine-containing stapled peptides. (a) [H_2N]-HG-X-ARA-X-GAD-[CO_2H]. (b) [H_2N]-HG-X-AOA-X-GAD-[CO_2H]. (c) [H_2N]-HG-X-RAA-X-GAD-[CO_2H]. (d) [H_2N]-HG-X-OAA-X-GAD-[CO_2H]. The "X" represents pentenyl alanine residues that have been stapled together through ruthenium catalyzed ring-closure metathesis. Unique fragment ions detected for the ornithine-containing peptides are indicated in red.

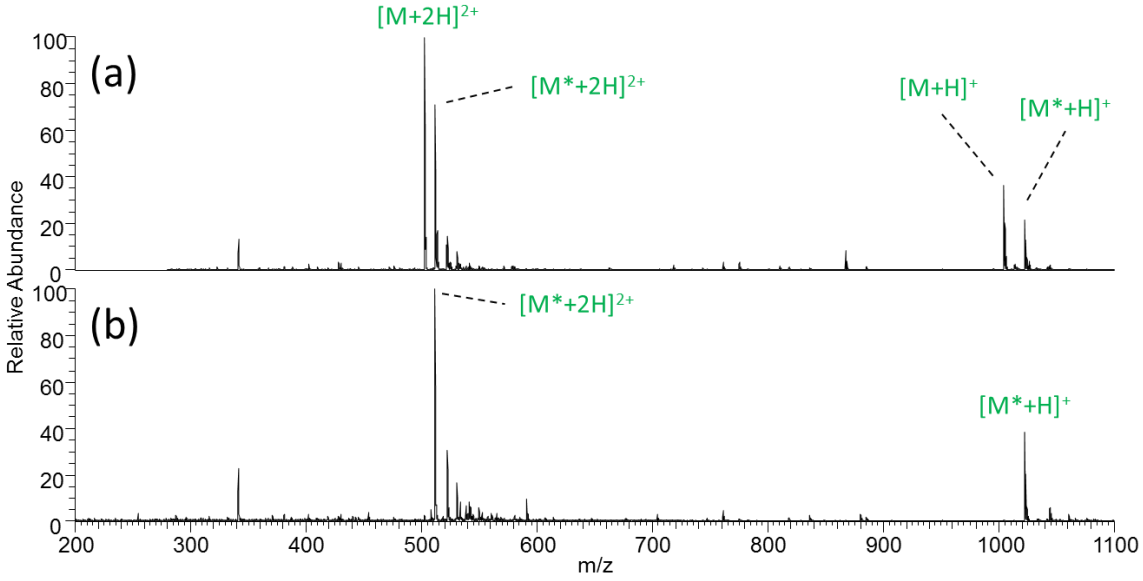

Figure 1.11. ESI mass spectrum of (a) unmodified stapled peptide [H2N]-HG-X-ARA-X-GAD-[CO2H] and (b) unmodified stapled peptide [H2N]-HG-X-RAA-X-GAD-[CO2H], both following trypsin digestion. An asterisk (*) represents presence of the tryptic product of the stapled peptides. The "X" represents pentenyl alanine residues that have been stapled together through ruthenium catalyzed ring-closure metathesis.

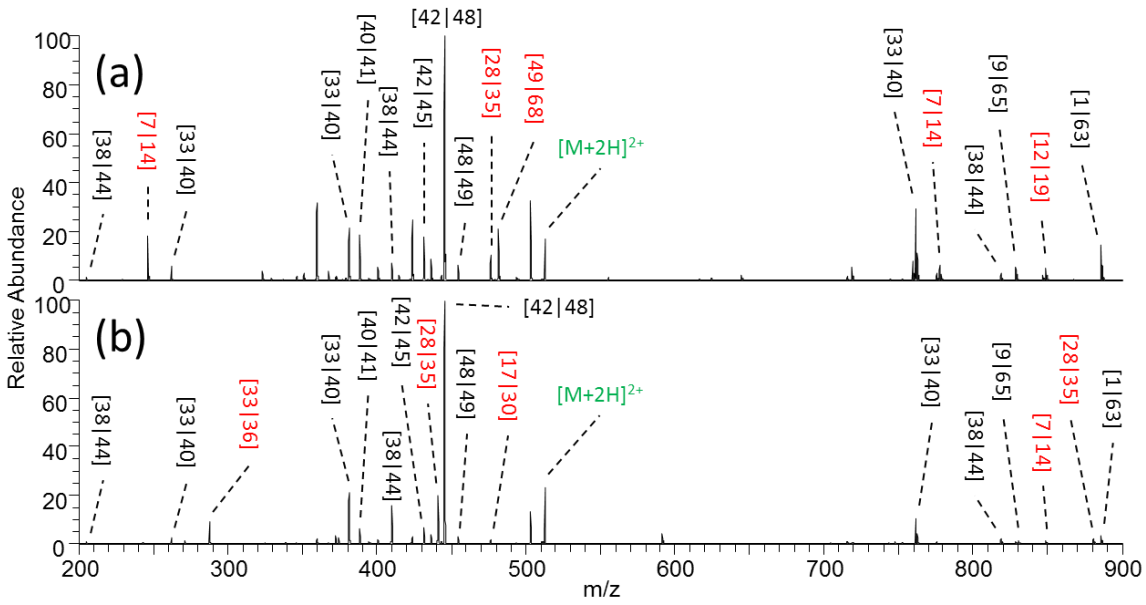

Figure 1.12. CID mass spectra (240K resolution) of 2+ unmodified stapled peptides after trypsin digestion. (a) [H2N]-HG-X-ARA-X-GAD-[CO2H]. (b) [H2N]-HG-X-RAA-X-GAD-[CO2H]. The "X" represents pentenyl alanine residues that have been stapled together through ruthenium catalyzed ring-closure metathesis. Red labels designate the unique fragment ions between the isobaric stapled peptides.

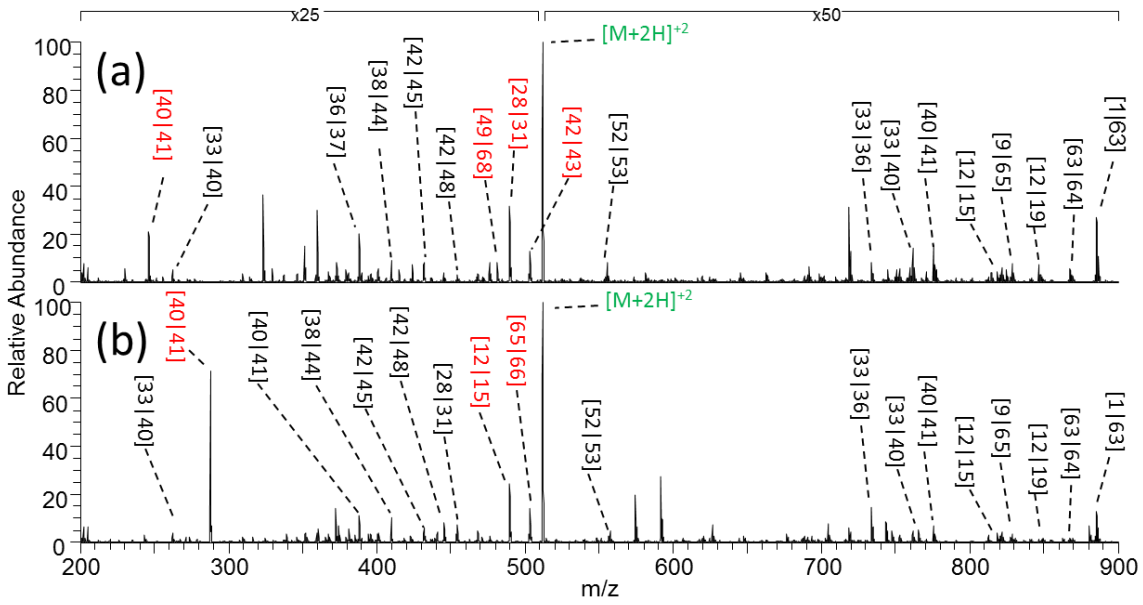

Figure 1.13. UVPD (2.5 mJ, 1 pulse) mass spectra (240K resolution) of 2+ unmodified stapled peptides after trypsin digestion. (a) [H2N]-HG-X-ARA-X-GAD-[CO2H]. (b) [H2N]-HG-X-RAA-X-GAD-[CO2H]. The "X" represents pentenyl alanine residues that have been stapled together through ruthenium catalyzed ring-closure metathesis. Red labels designate the unique fragment ions between the isobaric stapled peptides.

Sunflower trypsin inhibitor-1 (SFTI-1) is another prime candidate to evaluate the utility of the ornithine effect for improving the characterization of cyclic peptides. Similar to the hurdle with analysis of stapled peptides, two bond cleavages are required to generate diagnostic fragment ions for cyclic peptides like SFTI-1. The use of the custom algorithm to assign *m/z* values for all possible cross-ring cleavage products is vital for predicting and assigning fragment ions for SFTI-1. SFTI-1 has a single arginine residue within its cyclic structure, which, upon conversion to an ornithine group and activation in the gas phase, causes a ring opening event that exposes a significant portion of the molecule (**Figure 1.14**).

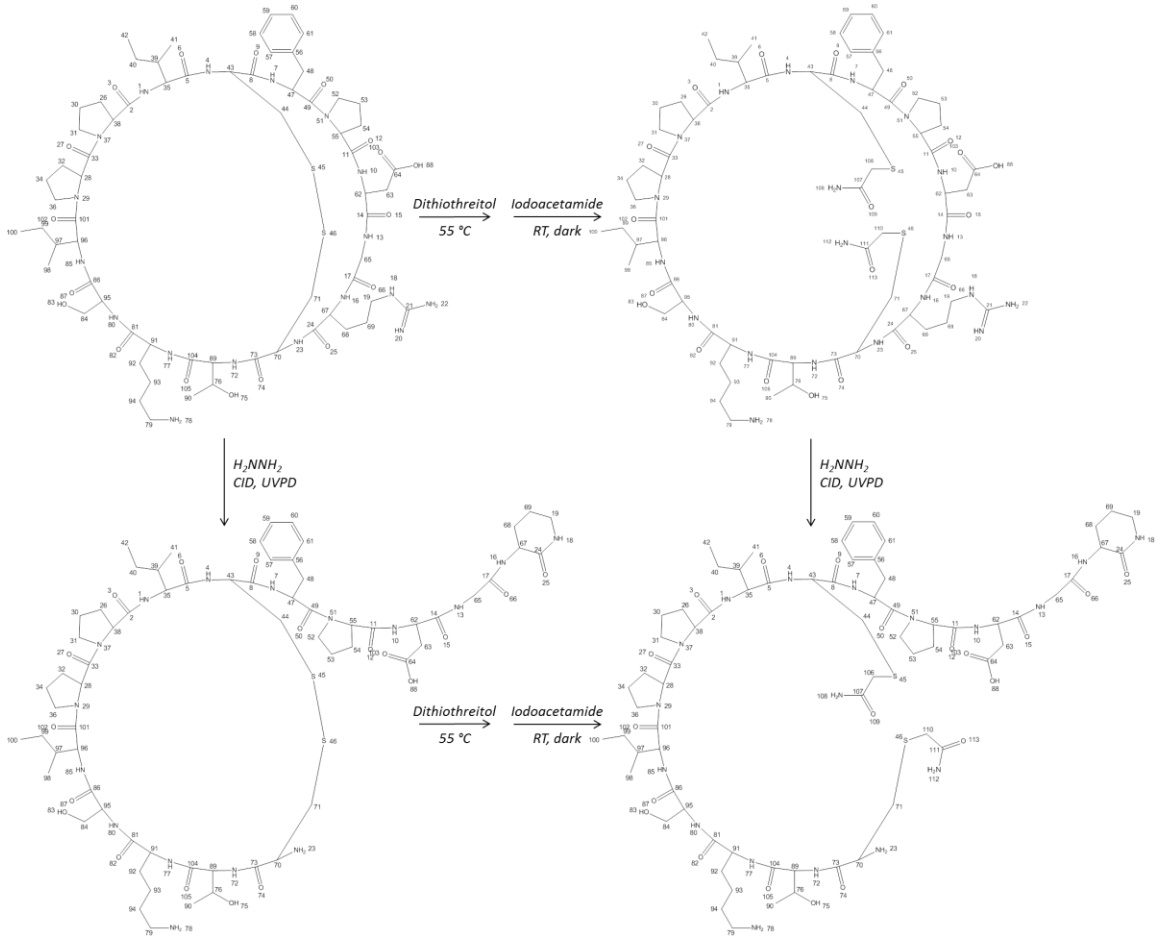

Figure 1.14. Sunflower Trypsin Inhibitor-1 (SFTI-1) may undergo a ring-opening event when the arginine residue is converted to ornithine followed by subsequent collision or photon-based activation. The ring can further be manipulated by reducing and alkylating the disulfide bond, allowing improved sequence coverage of the peptide backbone.

The arginine residue converts readily to an ornithine residue in the presence of hydrazine hydrate, as shown in the ESI mass spectrum (**Figure 1.15**). Furthermore, reduction and alkylation of the disulfide bond constraining the cyclic portion of the molecule was performed, allowing more extensive sequence coverage of the biomolecule. Upon CID (**Figure 1.16**) and UVPD (**Figure 1.17**), the greatest number of diagnostic

ions are produced and identified for the ornithine-modified peptide after reduction and alkylation (**Figure 1.16b** and **Figure 1.17b**). A complete list of the identified fragments and the associated m/z values are provided in **Table 1.1**, and the most prominent ones for the ornithinemodified SFTI-1 after reduction and alkylation are shown in **Figure 1.18**.

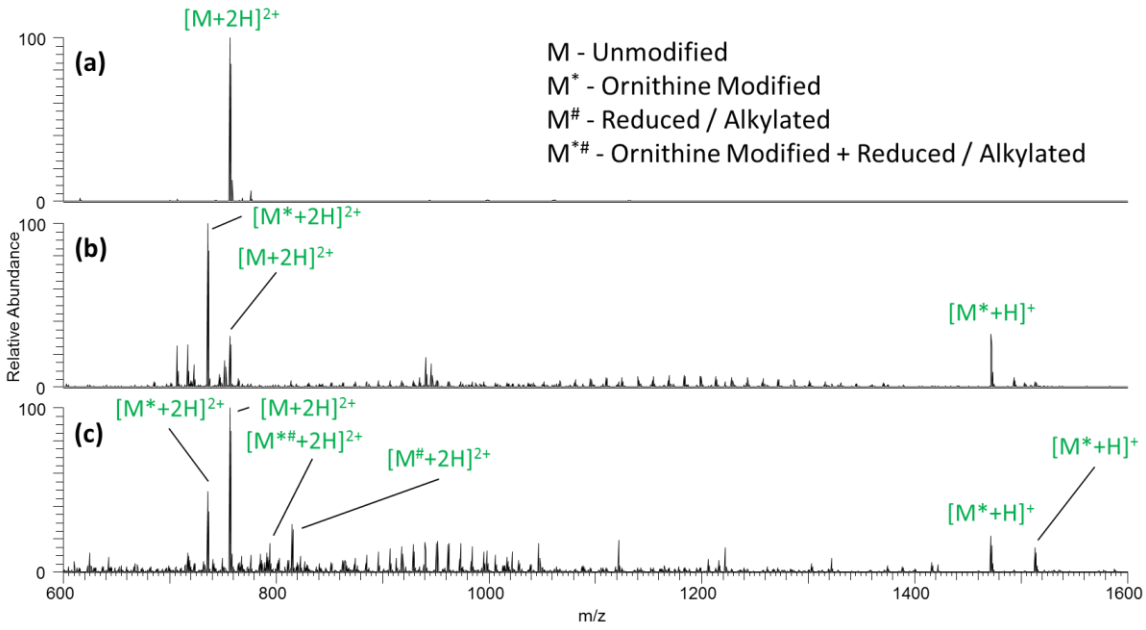

Figure 1.15. ESI mass spectra of (a) unmodified cyclic peptide SFTI-1, (b) ornithine-modified cyclic peptide SFTI-1, and (c) ornithine-modified cyclic peptide SFTI-1 after reduction and alkylation. An asterisk (*) represents presence of the modification from arginine to ornithine and a pound symbol (#) represents reduction and alkylation of a disulfide bond.

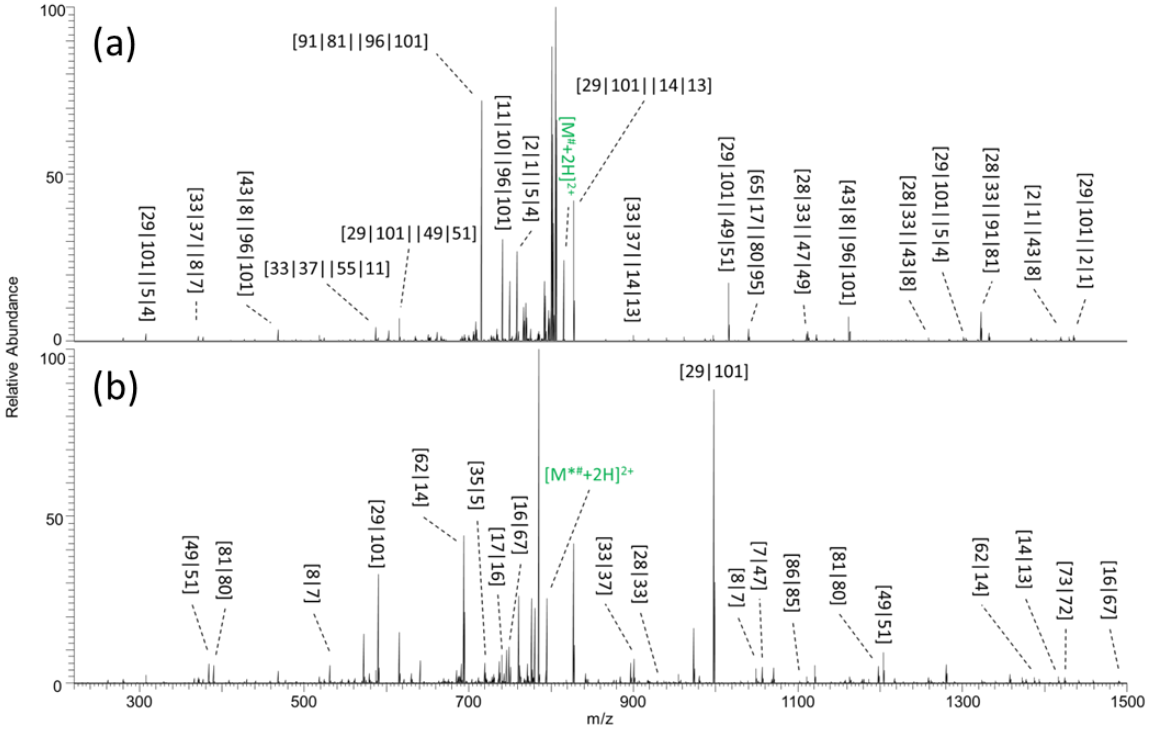

Figure 1.16. CID mass spectra (240K resolution) of doubly charged (a) reduced and alkylated unmodified SFTI-1 (1629.90 Da) and (b) reduced and alkylated ornithine-modified SFTI-1 (1587.86 Da). (NCE = 24) An asterisk (*) represents presence of the modification from arginine to ornithine and a pound (#) represents reduction and alkylation of the disulfide bond.

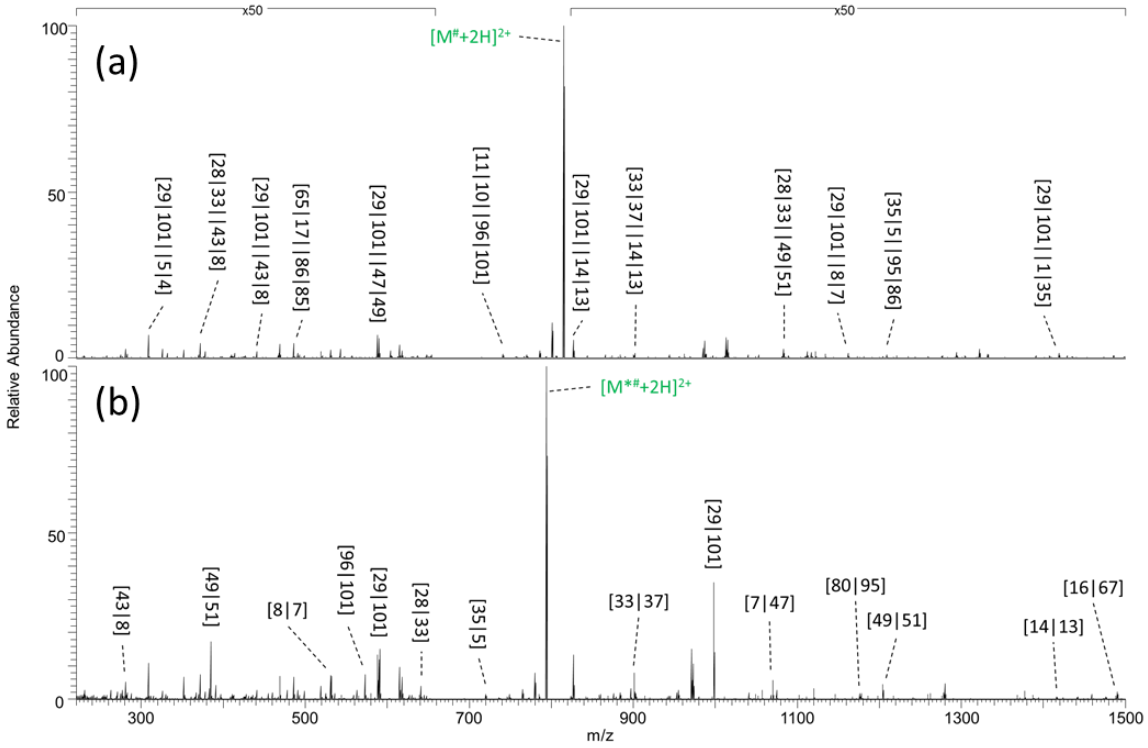

Figure 1.17. UVPD mass spectra (2.5 mJ, 1 pulse, 240K resolution) of doubly charged (a) reduced and alkylated unmodified SFTI-1 (1629.90 Da) and (b) reduced and alkylated ornithine-modified SFTI-1 (1587.86 Da). An asterisk (*) represents presence of the modification from arginine to ornithine and a pound (#) represents reduction and alkylation of the disulfide bond.

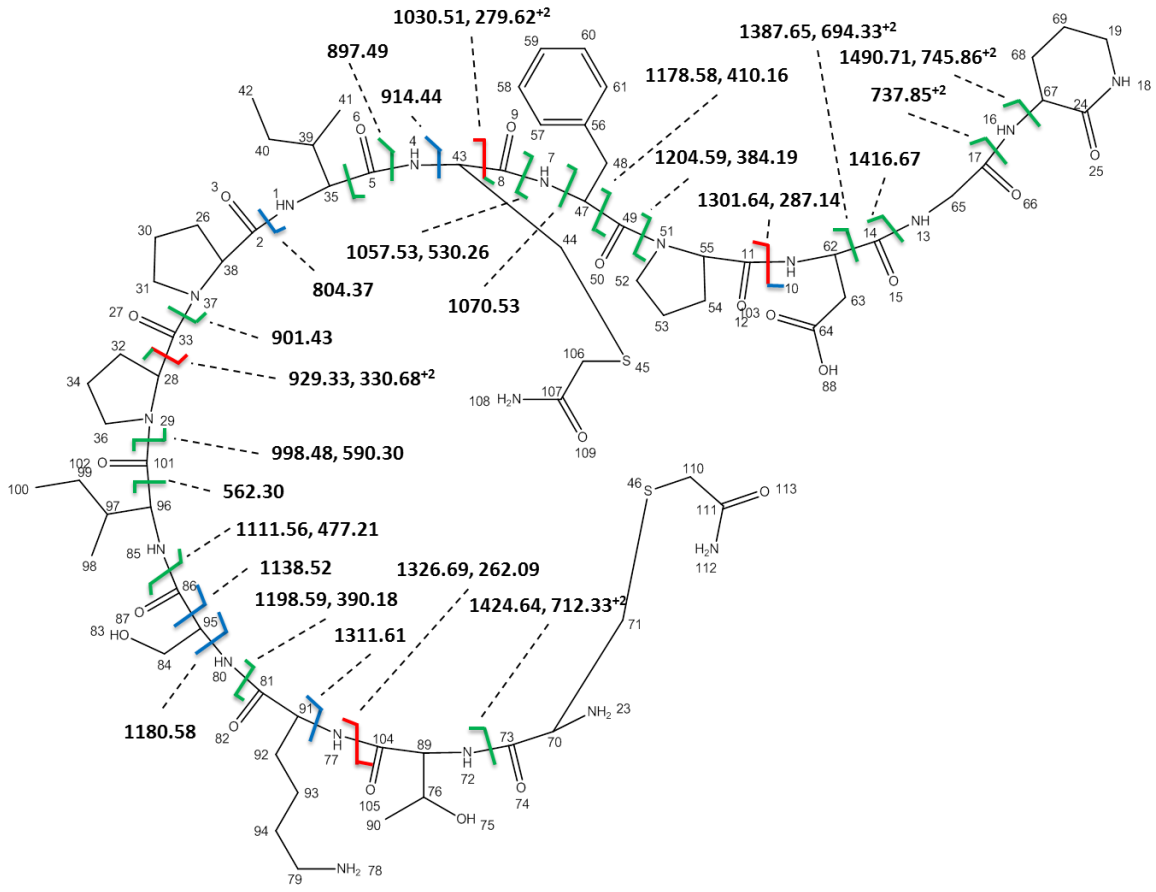

Figure 1.18. Fragmentation map of ornithine-modified SFTI-1 that has been reduced and alkylated. Red cleavages correspond to those fragment ions unique to CID; blue cleavages correspond to fragment ions unique to UVPD; green cleavages correspond to fragment ions produced by CID and UVPD.

Additionally, CID and UVPD of unmodified SFTI-1 and ornithine-modified SFTI-1 without reduction and alkylation were performed and the resulting spectra are shown in **Figure 1.19** and **Figure 1.20**, respectively. For comparison, a fragmentation map similar to **Figure 1.18** is provided for the unmodified SFTI-1 (i.e., reduced and alkylated, but without the ornithine modification) in **Figure 1.21**. Although there were still a number of fragment ions identified for unmodified SFTI-1 (reduced and alkylated

but without the ornithine modification), the ambiguity associated with the cyclic nature of the peptide impeded the assignment of product ions. In essence, several of the fragment ions may arise from multiple fragmentation points across the cyclic peptide, hence leading to the redundancies in **Table 1.1**. Owing to this ambiguity, exploiting the ornithine effect in tandem with reduction and alkylation leads to more confident characterization of the peptide.

As an alternative to the ornithinylation approach, tryptic proteolysis of SFTI-1 was undertaken. Tryptic digestion of SFTI-1, either with reduction/alkylation or without, failed to cause ring opening. Because SFTI-1 is a known trypsin inhibitor [51, 52], this result was not surprising and emphasizes the need for alternative approaches to facilitate the characterization of unusual peptides.

Table 1.1. Summary of fragment ions tabulated based on m/z ratios and bond cleavages for reduced and alkylated SFTI-1 (1629.90 Da, 2+ precursor selected) and ornithine-modified SFTI-1 that has been reduced and alkylated (1587.86 Da, 2+ precursor selected). In the instances when a single m/z value has multiple fragments listed next to it, this is due to multiple cross-ring cleavages that lead to the same m/z value.

SFTI-1 Reduce / Alkylate CID		SFTI-1 Orn Reduce / Alkylate CID		SFTI-1 Reduce / Alkylate UVPD		SFTI-1 Orn Reduce / Alkylate UVPD	
m/z	Fragment	m/z	Fragment	m/z	Fragment	m/z	Fragment
1435.68	29|101||2|1	1490.71, 745.86	16|67	1435.68	29|101||2|1	1490.71, 745.86	16|67
	38|2||96|101				38|2||96|101		
		1424.64, 712.33	73|72			1424.64, 712.33	73|72
1419.66	29|101||1|35			1429.65	29|101||81|80		
	28|33||35|5	1416.67	14|13		55|11||17|16	1416.67	14|13
	28|33||95|86				65|17||23|70		
	33|37||5|4	1387.65	62|14		77|91||86|85	1387.65	62|14
	33|37||86|85				91|81||96|101		
		1326.69, 262.09	77|104			1311.61	77|91
1383.66	2|1||43|8			1419.66	29|101||1|35		
		1301.64	11|10		28|33||35|5	1204.59, 384.19	49|51
1332.62, 661.8, 308.19	29|101||5|4				28|33||95|86		
	38|2||95|86	1204.59, 384.19	49|51		33|37||5|4	1198.59, 390.18	81|80
	2|1||86|85				33|37||86|85		
	1|35||85|96	1198.59, 390.18	81|80			1180.58	80|95
	35|5||96|101			1391.66	28|33||5|4		
		1178.58, 410.16	47|49		33|37||95|86	1178.58, 410.16	47|49
1259.62	28|33||43|8				1|35||96|101		
	33|37||8|7	1111.56, 477.21	86|85			1138.52	95|86
				1332.62, 661.8, 308.19	29|101||5|4		
1162.57, 468.22	29|101||8|7	1070.53	7|47		38|2||95|86	1111.56, 477.21	86|85
	43|8||96|101				2|1||86|85		
		1057.53, 530.26	8|7		1|35||85|96	1070.53	7|47
1112.55, 518.24	28|33||47|49				35|5||96|101		
	33|37||49|51	1030.51, 279.62	43|8			1057.53, 530.26	8|7
	38|2||55|11			1294.6	2|1||95|86		
	2|1||11|10	998.48, 590.30	29|101		35|5||49|51	998.48, 590.30	29|101
	1|35||10|62				5|4||96|101		

Table 1.1 (continued)

		929.33, 330.68	28|33			914.44	4|43
1040.5	29|101||24|23			1277.56	38|2||80|95		
	65|17||80|95	901.43	33|37			901.43	33|37
	67|24||96|101			1259.62	28|33||43|8		
		897.49	5|4		33|37||8|7	897.49	5|4
1015.5, 615.29	29|101||49|51						
	28|33||55|11	737.85	17|16	1209.51	35|5||95|86	804.37	2|1
	33|37||11|10				5|4||86|85		
	47|49||96|101	719.37	35|5		4|43||85|96	737.85	17|16
997.49	65|17||95|85	694.33	62|14	1162.57, 468.22	29|101||8|7	719.37	35|5
	17|16||86|85				43|8||96|101		
	16|67||85|96	562.3	96|101			694.33	62|14
				1134.57	38|2||77|104		
900.47	28|33||62|14					661.35	28|33
	33|37||14|13			1112.55, 518.24	28|33||47|49		
					33|37||49|51	562.3	96|101
827.37	29|101||14|13				38|2||55|11		
	33|37||16|67				2|1||11|10	287.14	11|10
	1|35||67|24				1|35||10|62		
	62|14||96|101					279.62	43|8
				1083.54	28|33||49|51		
758.86	29|101||86|85				38|2||11|10		
	38|2||35|5						
	2|1||5|4			1015.5, 615.29	29|101||49|51		
	1|35||4|43				28|33||55|11		
					33|37||11|10		
749.38	5|4||43|8				47|49||96|101		
740.38	38|2||23|70			987.51	28|33||11|10		
	11|10||96|101				49|51||96|101		
715.34	29|101||81|80			944.43	47|49||85|96		
	33|37||67|24						
	77|91||86|85			900.47	28|33||62|14		
	91|81||96|101				33|37||14|13		
651.29	29|101||77|104			827.37	29|101||14|13		
					33|37||16|67		

Table 1.1 (continued)

603.3	62|14||91|81		1|35||67|24
	14|13||81|80		62|14||96|101
	13|65||80|95		
		766.87	29|101||33|37
587.3	29|101||47|49		28|33||38|2
	33|37||55|11		33|37||2|1
377.22	43|8||77|91	758.86	29|101||86|85
			38|2||35|5
371.17	28|33||43|8		2|1||5|4
	33|37||8|7		1|35||4|43
		740.38	38|2||23|70
			11|10||96|101
		715.34	29|101||81|80
			33|37||67|24
			77|91||86|85
			91|81||96|101
		682.36	7|47||81|80
		603.3	62|14||91|81
			14|13||81|80
			13|65||80|95
		587.3	29|101||47|49
			33|37||55|11
		542.27	10|62||89|104
			23|70||96|101
		530.28	7|47||67|24
			16|67||81|80
		485.26	38|2||14|13
			65|17||86|85
		440.23	29|101||43|8

Table 1.1 (continued)

	377.22	43|8||77|91
	371.17	28|33||43|8
		33|37||8|7

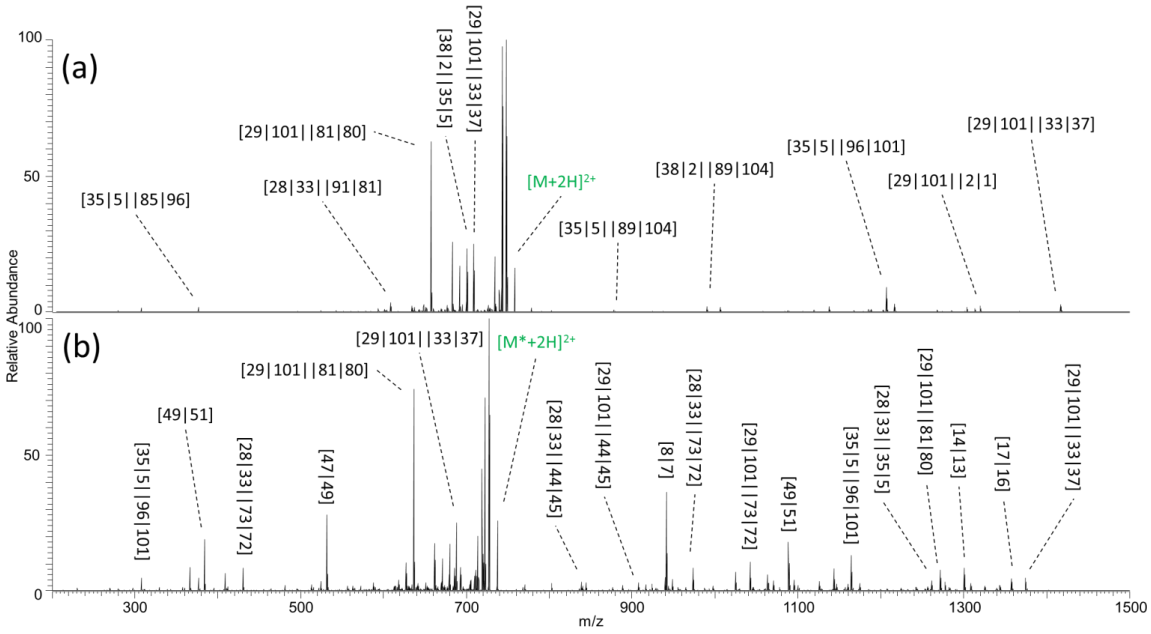

Figure 1.19. CID mass spectra (240K resolution) of doubly charged (a) unmodified SFTI-1 (1513.60 Da) and (b) ornithine-modified SFTI-1 (1471.60 Da). (NCE = 24) An asterisk (*) represents presence of the modification from arginine to ornithine.

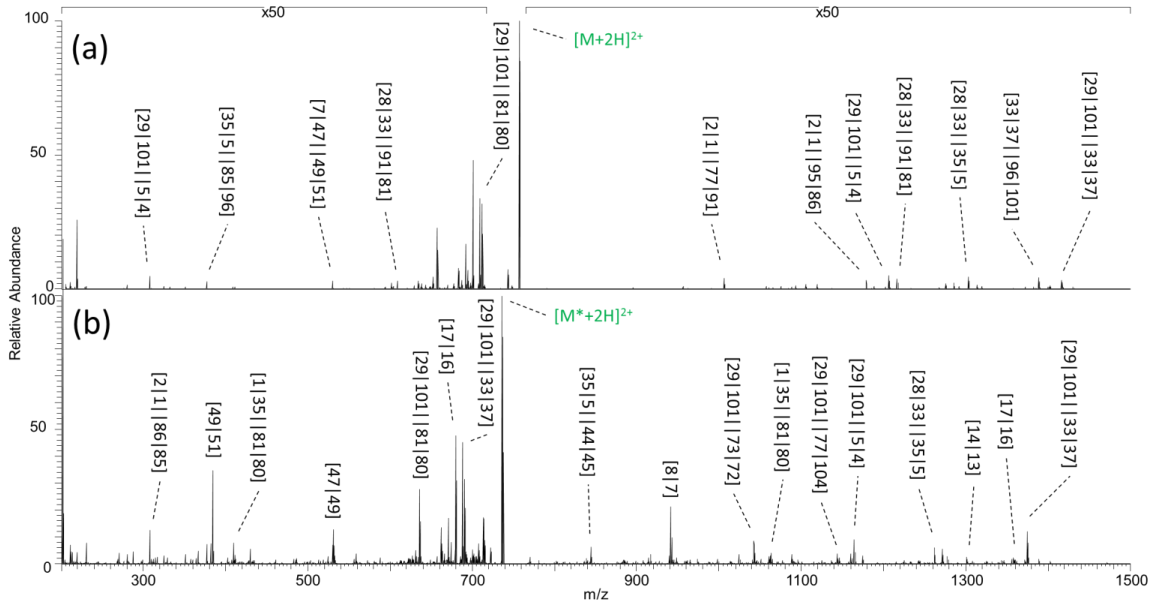

Figure 1.20. UVPD mass spectra (2.5 mJ, 1 pulse, 240K resolution) of doubly charged (a) unmodified SFTI-1 (1513.60 Da) and (b) ornithine-modified SFTI-1 (1471.60 Da). (NCE = 24) An asterisk (*) represents presence of the modification from arginine to ornithine.

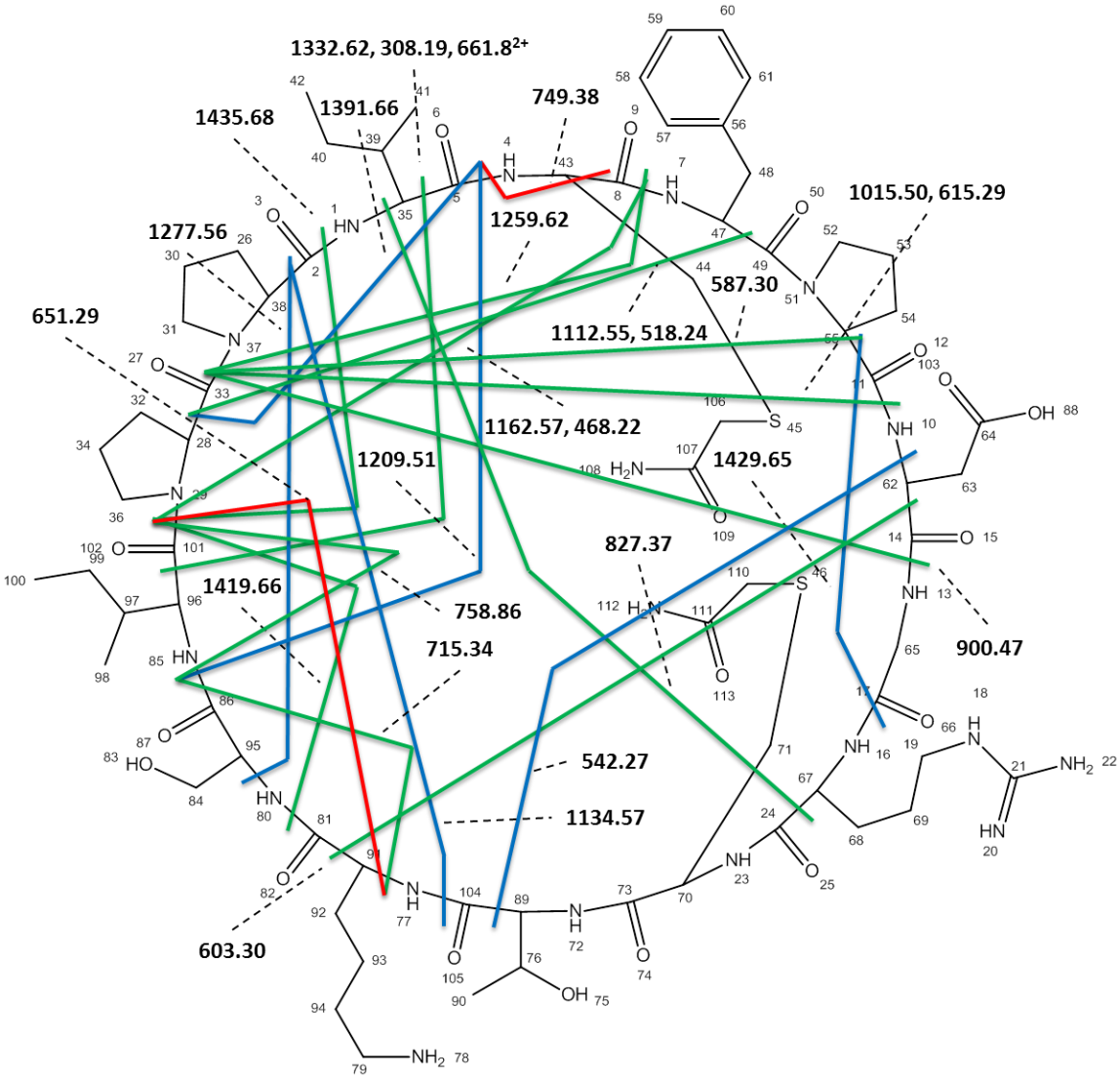

Figure 1.21. Fragmentation map of unmodified SFTI-1 that has been reduced and alkylated. Red cleavages correspond to those fragment ions unique to CID; blue cleavages correspond to fragment ions unique to UVPD; green cleavages correspond to fragment ions produced by CID and UVPD. (note: not all fragment ions are displayed, please see **Table 1.1** for a full list of all identified fragment ions).

CONCLUSIONS 1.5

Conversion of arginine residues to ornithine residues provided an effective way to promote ring opening reactions of stapled or cyclic peptides chemically rather than enzymatically, with greater specificity than tryptic digestion. The preferential heterolytic cleavage C-terminal to the ornithine residue upon activation led to an N-terminal ion that terminated with a sixmembered lactam ring. The ornithine effect allowed characterization of isomeric stapled peptides as well as the cyclic peptide SFTI-1 upon CID or UVPD. A custom algorithm was developed to facilitate assignment of mass values to all possible fragment ions created upon cleavage of two bonds, including cross-ring cleavages. Use of this algorithm simplified the interpretation and assignment of fragment ions produced from cyclic peptides.

Chapter Two: Energy Resolved Mass Spectrometry of Lipid A Variants by Multiple MS/MS Techniques

OUTLINE 2.1

Lipid A molecules consist of a diglucosamine sugar backbone with a number of acyl chains which vary in their length and connectivity. Because of the challenging nature of characterizing these molecules and differentiating between isomeric species, an energy-resolved MS/MS strategy was undertaken to track the fragmentation trends and map genealogies of product ions originating from consecutive cleavages of acyl chains. Ten lipid A molecules were analyzed via this energy- resolved MS^2 approach. Generalizations were developed based on the number and locations of the primary and secondary acyl chains as well as variations in preferential cleavages arising from the location of the phosphate groups.

INTRODUCTION 2.2

Gram-negative bacteria are responsible for a variety of food-borne illnesses, respiratory and urinary tract infections, sexually transmitted diseases, and highly aggressive immune responses which can be fatal if proper treatment is unavailable [53–56]. The outer membrane of these bacteria contains a structurally complex lipopolysaccharide (LPS) responsible for many of their infectious and toxic properties [57, 58]. LPS is structurally organized into three unique, covalently linked regions which extend from the surface of the bacterial membrane [59]. At the exterior is a highly variable polyglycan O-antigen region, connected to a non-repeating saccharide core,

followed by a hydrophobic domain known as lipid A, which is responsible for fastening LPS to the membrane surface [60, 61].

The sugar backbone of lipid A is highly conserved in most bacteria, comprised of two pyranosidic hexosamine residues as β(1,6)-linked glucosamine dimers. Branching from this central motif are a series of highly variable (R)-3-hydroxy acyl groups linked at the N-2, O-3, N-2' and O-3' positions by ester or amide bonds [62]. Owing to random mutations along with certain modulating environmental factors, the length and number of acyl chains extending from the sugar backbone of lipid A varies across bacterial species [63]. One or two phosphates are usually found at the 1’ and 4’ carbon positions of the diglucosamine backbone, occasionally with variable substituents including glycans and phosphoethanolamine [64]. One example of this structural variability is found in the lipid A of *P. aeruginosa* bacteria isolated from the airways of cystic fibrosis patients [65,66]. The lipid A found in the clinical isolates incorporated both a palmitate moiety and an aminoarabinose group and retained a C10 fatty acid, all specific modifications not found in other strains of *P. aeruginosa*, a finding that suggested unique adaptation of the bacteria in a way that may contribute to antimicrobial resistance [65,66]. Currently, our understanding of the structural changes of lipid A and the way in which they help impart antibiotic resistance and recognition failure by the immune system is limited. As a result, it is imperative that efficient and reliable methods be developed to improve analysis of this diverse structure.

Currently, most mass spectrometry-based lipid analyses rely on MS/MS in order to generate fragmentation profiles for structural characterization. Collision induced

dissociation (CID) and high-energy collisional dissociation (HCD) have been particularly useful in generating fragment libraries necessary for accurate profiling of different lipid A variants [65–73]. An alternative to collision-based methods for ion activation/fragmentation is ultraviolet photodissociation (UVPD) [74–76]. As shown previously, UVPD results in structure-specific glycosidic and cross-ring fragments of lipid A and affords richer fragmentation patterns when compared to conventional collisional activation methods [77–85]. Recent work by the Goodlett group successfully determined the structures of various lipid A using an automated hierarchical tandem MS algorithm known as HitMS [86]. This profiling method interrogated diagnostic fragment ions and neutral losses across MSn events by aligning each fragment (based on *m/z* value) with its most probable structure. We envisioned that a combination of MS^n and energy-variable MS/MS strategies, ideally coupled with powerful algorithms like HitMS, could further facilitate characterization of lipid A and assignment of structures. In order to overcome some of the experimental and data processing obstacles encountered in current lipid A studies, our group recently demonstrated a hierarchical method, UVliPiD, for identification of acyl chain linkages in bis-phosphoryl lipid A structures [87]. Following fragmentation of lipid A by an initial stage of UVPD, the resulting charge-reduced photodetachment products were subjected to secondary activation using CID without isolation of specific intermediates. However, the rather naïve guesswork of this decision-based approach spurred our interest in refining the method by incorporating specific predictive rules based on monitoring the fragmentation pathways as a function of energy deposition.

In recent years, energy-resolved mass spectrometry (ERMS) has proved to be a valuable technique for mapping complex oligosaccharides and other biopolymers based on trends in fragmentation relative to internal energy deposited during the activation event [30, 31]. Even for molecules that generate the identical sets of fragment ions upon MS/MS, ERMS may allow an opportunity to differentiate isomers based on variations in the fragmentation trends as a function of energy. Here we use energy-variable HCD, CID, and UVPD to compare the preferred fragmentation pathways and map the genealogies of fragmentation of a series of lipid A molecules in an effort to develop rules for predicting lipid A fragmentation patterns and to facilitate development of fragment ion assignment algorithms. HCD proved to be particularly useful for tracking secondary or consecutive fragmentation routes. Further, changes in phosphorylation appeared to cause predictable variations in specific dissociation events.

EXPERIMENTAL 2.3

Synthetic monophosphoryl lipid A (MPLA), synthetic monophosphoryl 3-deacyl lipid A (MP3DALA), and detoxified monophosphoryl lipid A (DMPLA) from *Salmonella minnesota R595* were purchased from Avanti Polar Lipids (Alabaster, AL) and used without further purification. *E. coli* bis-phosphorylated lipid A was purchased from Sigma-Aldrich (St. Louis, MO) and also used without further purification. Additionally, lipid A variants were isolated and purified from *E. coli* expressing LpxJ from *C. jejuni*, from *Acinetobacter baumannii*, from *W. succinogenes*, and from *E. coli* strain BN2, as described previously [83, 90, 91]. HPLC grade chloroform, methanol, and water used during sample preparation were purchased from EMD Millipore (Billerica,

MA). Manual determination of fragment ions was accomplished using the ChemDraw software suite (Perkin Elmer, Waltham, MA).

All lipid A samples used in this study were dissolved in 74:23:3 chloroform:methanol:water with final concentrations of 10 μM followed by analysis using both a Thermo Scientific Velos Pro dual linear ion trap and a Thermo Scientific Orbitrap Fusion mass spectrometer (San Jose, CA). Both mass spectrometers were equipped with a 193 nm excimer laser (Coherent, Santa Clara, CA) to perform photodissociation, as previously described [77, 92]. Static emitters were used to transport lipid A molecules into the gas phase via a 1.5 mm o.d. glass capillary pulled to a tip of less than 1 μm by a Sutter Instrument P2000 laser puller (Novato, CA). Solutions of the lipid A molecules were loaded into the pulled glass capillary and a platinum wire was inserted, generating ions when a potential of 1000-1500 V was applied to the wire. All experiments were conducted in the negative ion mode on the mass spectrometer, and CID, HCD, and UVPD were manually stepped to generate ERMS plots for the MS2 spectra. CID and HCD were stepped from NCE 0-50 in increments of 5 NCE, and UVPD was stepped in both energy (0-4 mJ, in 0.5 mJ increments) and pulses (1-11 pulses, in 2 pulse increments). For high resolution data collection on the Orbitrap Fusion mass spectrometer, a resolution of 120 K was used and a signal-to-noise threshold of 3 was used in analyzing the deconvoluted data in Xtract.

RESULTS AND DISCUSSION 2.4

ESI of lipid A species resulted in production of singly or doubly deprotonated species depending on whether the lipid A possessed one or two phosphate groups. HCD

and UVPD were used to characterize the deprotonated species in an energy variable manner to obtain information about the dominant fragmentation pathways and their genealogies as a function of energy deposition. ERMS plots were generated via variation of the collision energy for HCD or the number of laser pulses for UVPD. The ERMS plots give insight into the variations in fragment ion distributions as a function of energy deposition, thus providing a convenient way to track the conversion of primary fragment ions into secondary fragment ions and reveal the relative labilities of the acyl chains and the sequential order in which they are lost. For the results shown, fragmentation nomenclature from Domon *et al.* [93] and Morrison *et al.* [87] is adopted. All lipid A variants used in this study are shown in **Figure 2.1** and listed with their neutral masses and abbreviations used henceforth.

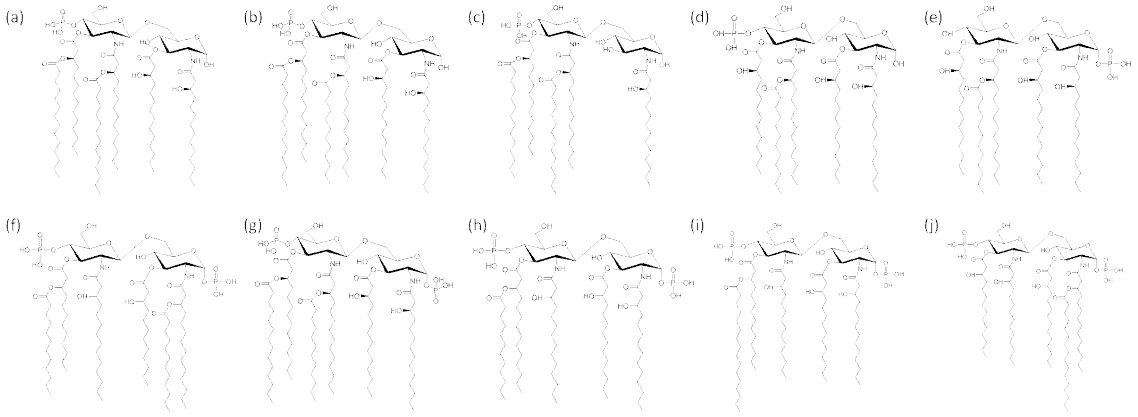

Figure 2.1. Supplementary Figure S1: All 10 lipid A variants evaluated. (a) monophosphoryl lipid A (1745.28 Da, lAA); (b) detoxified lipid A (1717.25 Da, lAB); (c) monophosphoryl 3-deacyl lipid A (1519.09 Da, lAC); (d) *E. coli* strain BN2E (1507.05 Da, lAD); (e) *E. coli* strain BN2F (1507.05 Da, lAE); (f) *Acinetobacter baumannii* expressing lpxL (1713.13 Da, lAF); (g) bisphosphorylated lipid A (1797.22 Da; lAG); (h) *W. succinogenes* lpxJ (1587.02 Da, lAH); (i) *C. jejuni* 240 0482 (1643.08 Da, lAI); (j) *C. jejuni* lpxJ (1643.08 Da, lAJ)

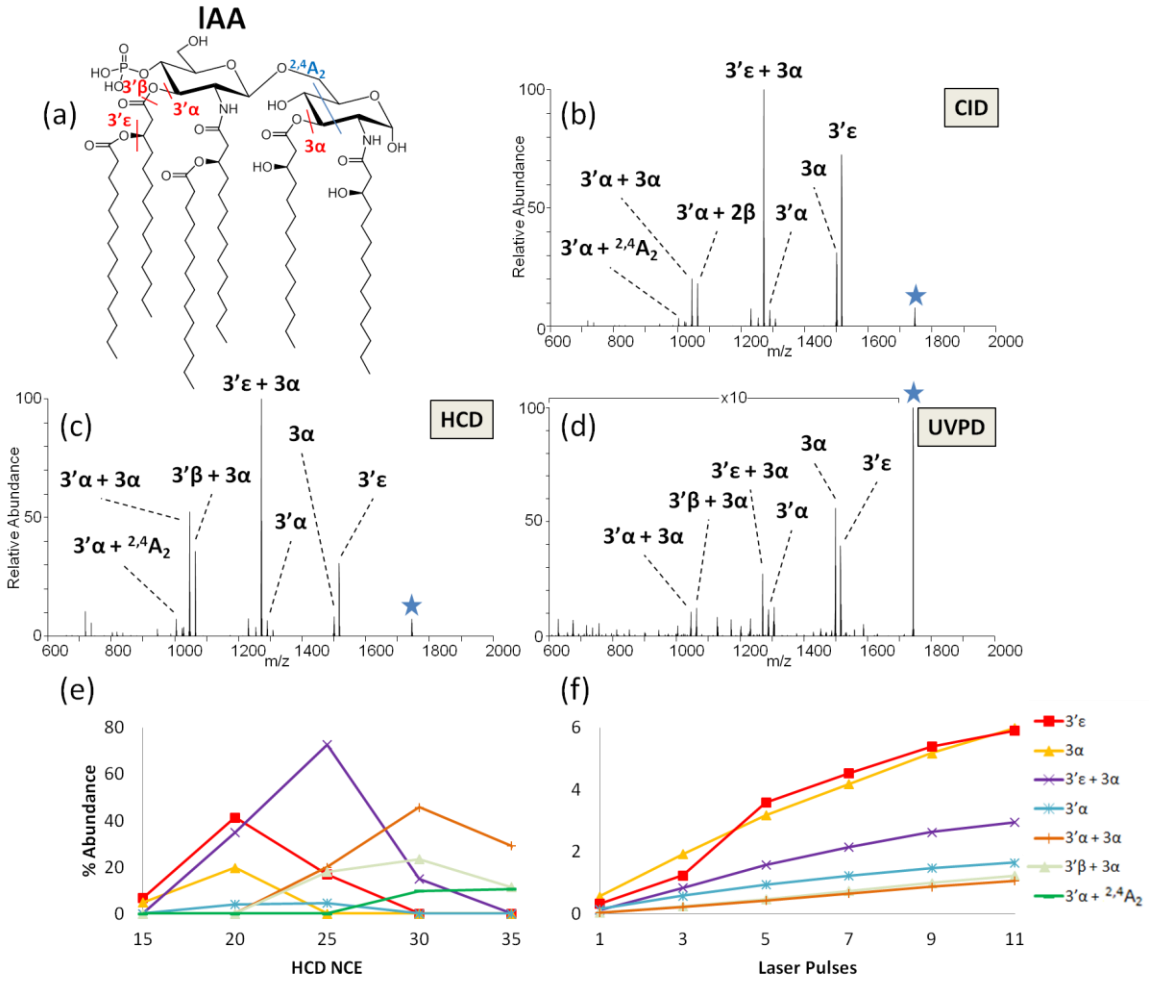

Figure 2.2. (a) Structure of monophosphoryl lipid A (monoisotopic mass 1745.3 Da) and the corresponding MS/MS spectra of the deprotonated lipid by: (b) CID at NCE 35, (c) HCD at NCE 25, and (d) UVPD at 2.5 mJ for seven pulses. Only the most prominent fragment ions are labelled. ERMS plots are shown in (e) HCD and f) UVPD.

As a representative example, lAA was analyzed via CID, HCD, and UVPD in an energy-variable method. The phosphate moiety is located on the non-reducing glucosamine, and this lipid A contains four primary acyl chains (at the 3', 2', 3, and 2 positions) as well as two secondary acyl chains of equal length located at the 3'- and 2'-

positions (**Figure 2.2a).** The corresponding CID, HCD, and UVPD spectra are shown in **Figure 2.2b, 2.2c**, and **2.2d**, respectively, and the companion energy-variable curves are shown in **Figure 2.3** (CID), **2.2e** (HCD), and **2.2f** (UVPD). The most dominant fragment ions identified resulted from losses of primary and secondary acyl chains at the 3'α, 3'ε, 3α, and 3'β positions (all of which are labelled on the structure in **Figure 2.2a**). There was also one cross-ring cleavage ($^{2,4}A_2$) that occurred on the unphosphorylated glucosamine. The MS/MS spectra revealed that the various acyl chains were cleaved individually (cleavage at 3'ε, 3α or 3'α) or as paired combinations (cleavage at 3'ε with 3α; or loss of 3α with 3'α or 3'β or 3'ε; or loss of 3'α with 3α or with cross-ring cleavage $^{2,4}A_2$). For HCD, the 3'ε and 3α cleavages were observed at the lowest onset energies. As the HCD energy was increased, the primary fragments originating from these cleavages were depleted, and new secondary fragment ions appeared, including ones attributed to cleavages of 3'ε + 3α and 3'α + 3α. The cleavage of the 3'α chain appeared at 20 NCE, along with secondary products due to sequential cleavages: 3'α + 3α and 3'α + $^{2,4}A_2$. Interestingly, the 2' and 2 acyl chains were never cleaved individually nor in tandem with any other acyl chain. Closer inspection of the energy-variable HCD and UVPD curves in **Figure 2.2e** and **2.2f** illustrates that the onsets for sequential fragmentation pathways were well-demarcated for HCD, whereas the onsets were identical for virtually all of the fragmentation pathways upon UVPD, including both cleavages of individual acyl chains and pairs of acyl chains. This behavior reflects the high internal energy deposition upon absorption of one or more UV photons and ultimately provides little genealogical information about fragmentation of lipid A. This type of energy-variable UVPD plot is

consistent for other lipid A, and thus the remainder of the study will focus on the energy-variable HCD curves which more clearly illustrate the step-wise nature of lipid A fragmentation. In direct comparison to the results obtained from the energy-variable analysis of lAA, the fragmentation preferences via HCD for lAB are shown schematically in **Figure 2.4**. Similarly to lAA, lAB (which has the same acyl chain connectivity, the only difference being the length of the 2'ε chain) demonstrates initial losses of the 3'ε and 3α acyl chains, followed by loss of the 3'α acyl chain and combinations of losses at 3'ε + 3α, 3'β + 3α, 3'α + 3α, and 3'α + $^{2,4}A_2$. The corresponding energy variable HCD and UVPD plots for lAB is shown in **Figure 2.5** and **Figure 2.6**.

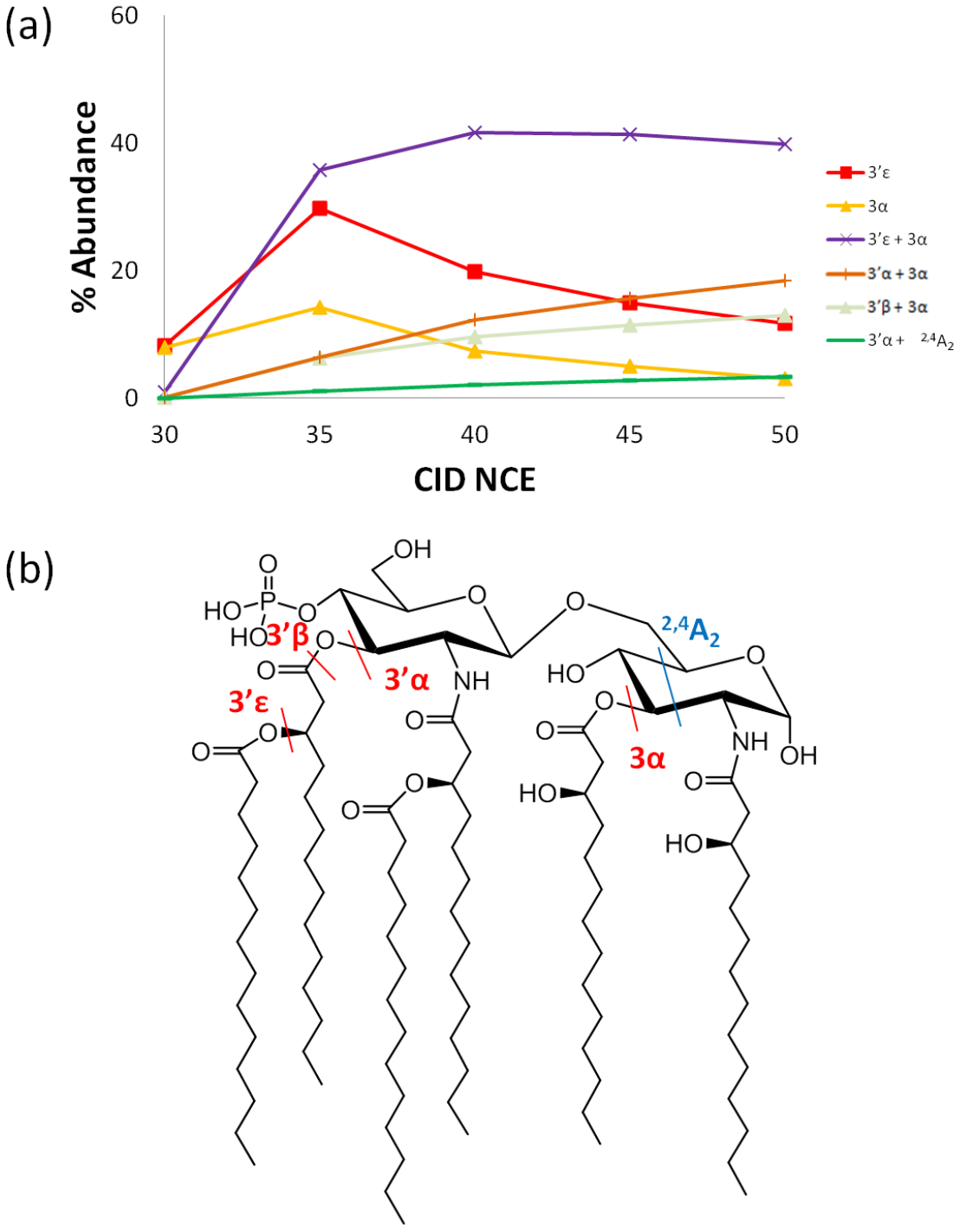

Figure 2.3. (a) CID ERMS of lAA and (b) the structure. CID ERMS does not afford the same genealogical information that HCD and UVPD do.

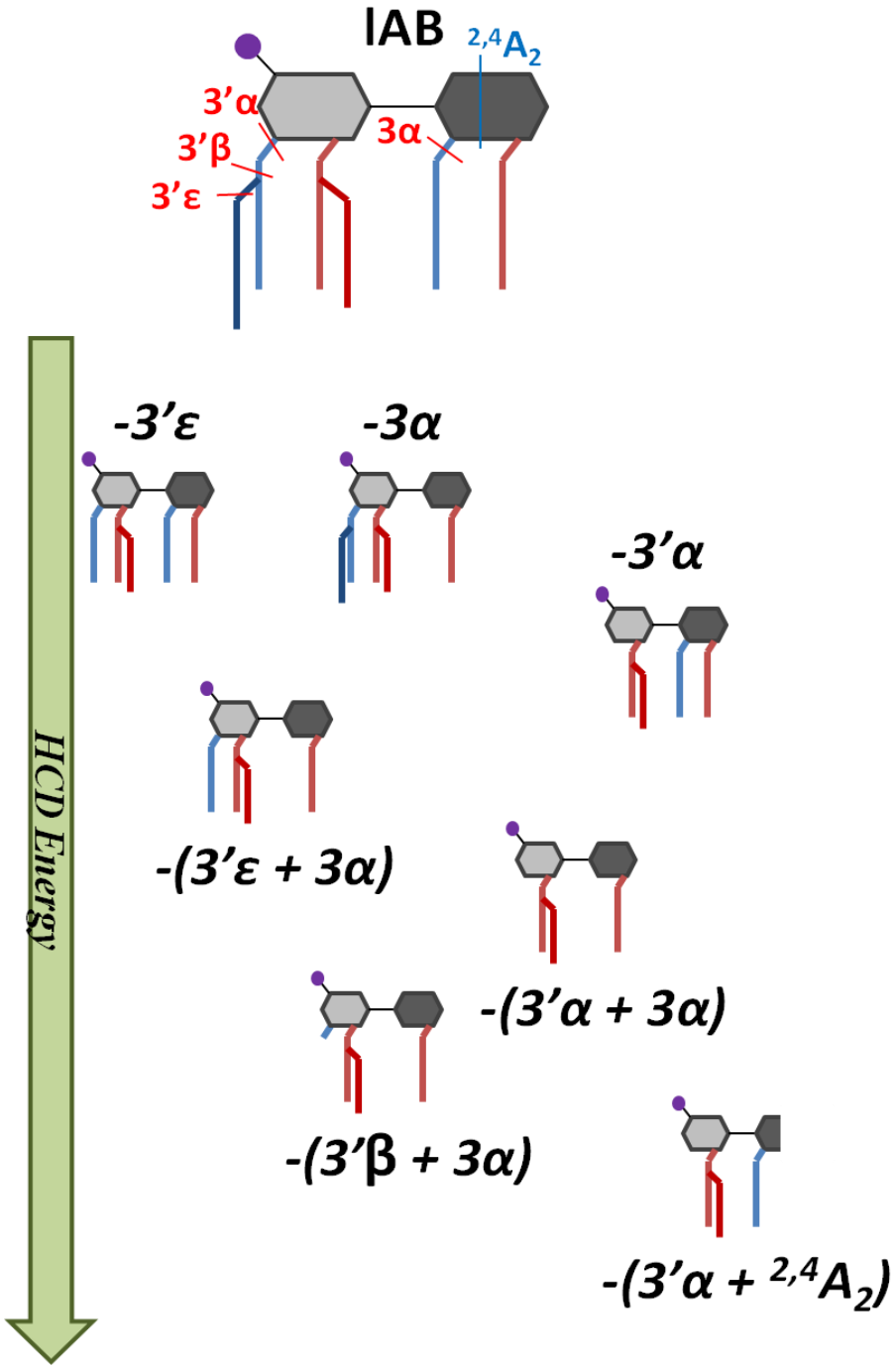

Figure 2.4. Illustration demonstrating the sequential fragmentation of lAB under ramped HCD energy.

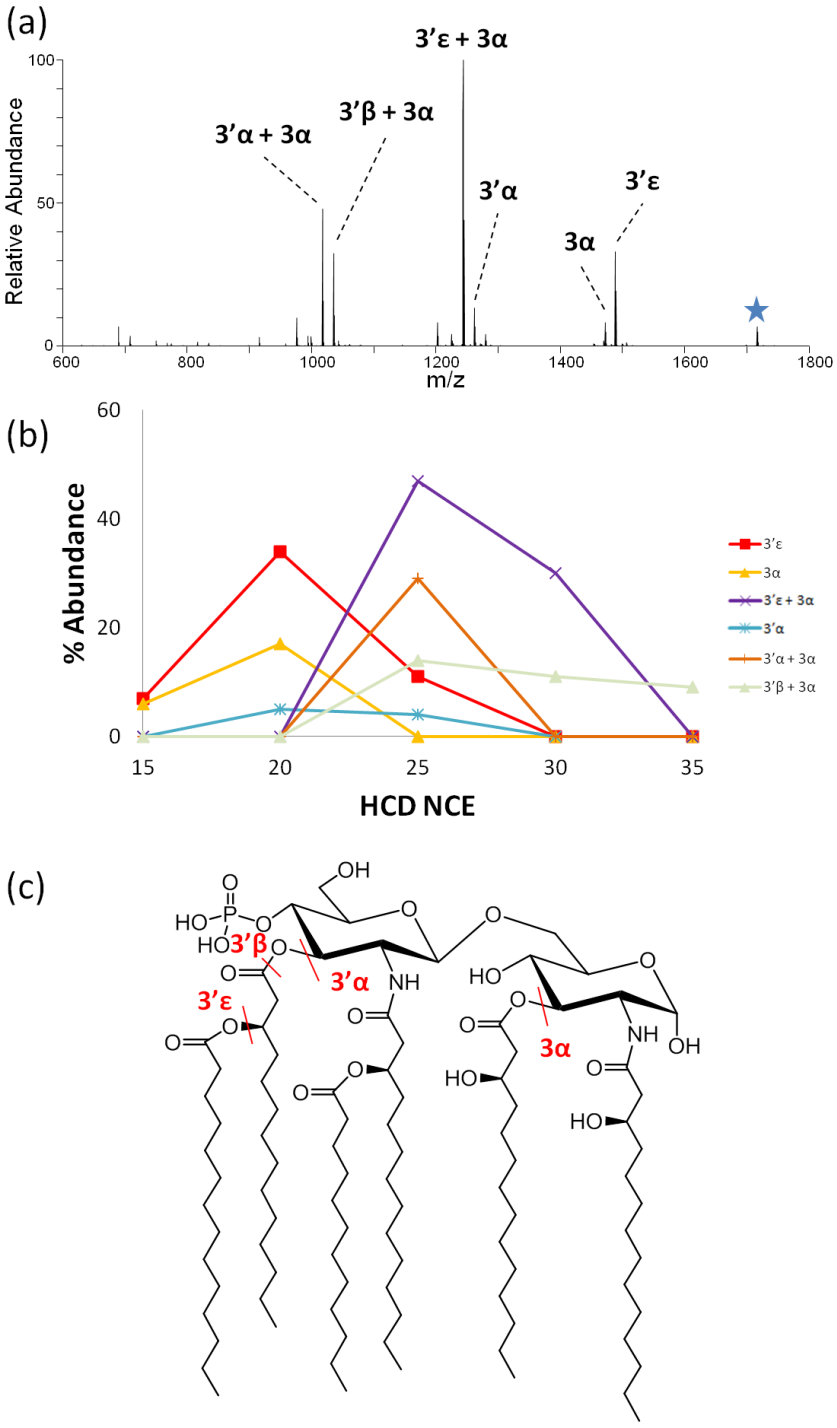

Figure 2.5. lAB MS2 spectra using HCD at NCE=25 (a) and the corresponding HCD ERMS plot (b). The structure of lAB is shown in (c).

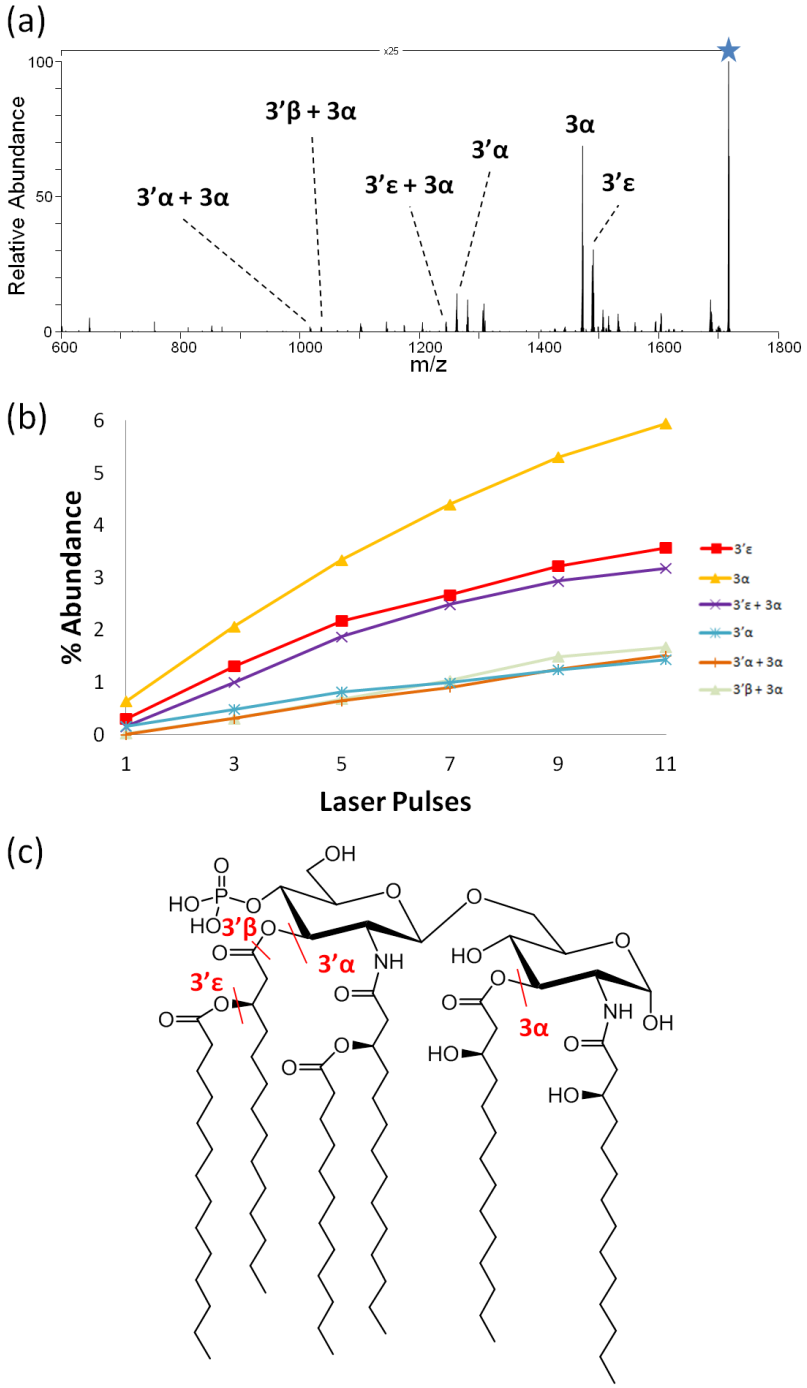

Figure 2.6. lAB MS2 spectra using UVPD at 3mJ, 5 pulses (a) and the corresponding UVPD ERMS plot (b). The structure for lAB is shown in (c).

Energy variable HCD was used to examine the impact of the acyl chains on the preferential cleavages at different positions. The resulting plots are shown for three monophosphoryl lipid A in **Figure 2.7** (as well as lAA in **Figure 2.2** and lAB in **Figure 2.5**), with the identified acyl chain and cross-ring cleavages mapped on each structure. The lipids in **Figure 2.7** all have five acyl chains; two are isomers. All five mono-phosphorylated lipid A included in this have a secondary acyl chain at the N-2' position; both lAA and lAB have an additional secondary acyl chain at the O-3' position. Upon comparison of the ERMS curves, it is clear that the presence of secondary acyl chains significantly modulates the fragmentation patterns owing to their lability upon activation of lipid A. Cleavage of the secondary acyl chain at the O-3' position (3'ε) is particularly favored, thus representing a dominant fragmentation observed at the lowest HCD energies. Loss of the O-3' secondary chain may occur in conjunction with cleavages of other acyl chains at higher collision energies, as evidenced by the trends for loss of 3'ε + 3α for lAC, lAA, and lAB. For lAD and lAE which lack the 3' secondary chain, cleavage of the secondary acyl chain at the 2' position (2'ε) is preferred. For all of the monophosphoryl lipid A, cleavages of the 3' and 3 acyl chains are prominent, either alone at the lower collision energies or in conjunction with additional acyl chain cleavages at higher collision energies. The higher energy onset of the combined loss of the acyl chains at the 3' and 3 positions suggests that loss of the 3' chain occurs first, followed by the acyl chain at the 3 position. In contrast to the trends observed for lAA for which there was an abundant ion attributed to cleavage of the 3'ε and 3α positions simultaneously (**Figure 2.2e**), this pathway is not highly favored for lAC and instead

cleavage of the 3’ chain (3’ε) in conjunction with cross-ring cleavage of the reducing end sugar ($^{2,4}A_2$) is favored (**Figure 2.7d**). This observation is particularly useful for structural elucidation of the acyl chain positions of lipid A. While the secondary 3’ chain was not present for the other two monophosphoryl lipid A structures, lAD and lAE, they still exhibited combinatorial losses of acyl chains as a function of increasing collisional energy. lAD favored initial cleavage at the 3’α position, whereas lAE favored cleavage at the 2’ε position. Both of these monophosphoryl lipid A isomers exhibited similar 2’ε and 3’α cleavages in conjunction with the acyl chain at the 3-position (α and β cleavages) (**Figure 2.7e, f**). The raw HCD spectrum for lAC at NCE=20 is shown in **Figure 2.8**.

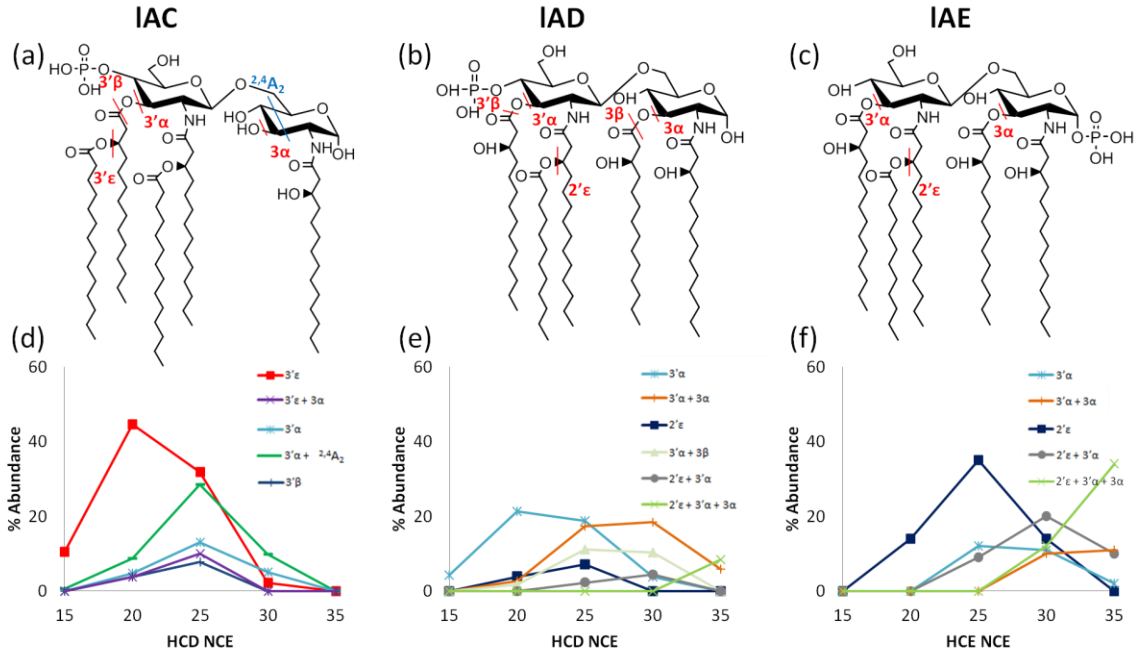

Figure 2.7. lAC, lAD, and lAE structures with key cleavage sites indicated (a, b, c) and respective HCD ERMS plots (d, e, f) for the deprotonated lipids.

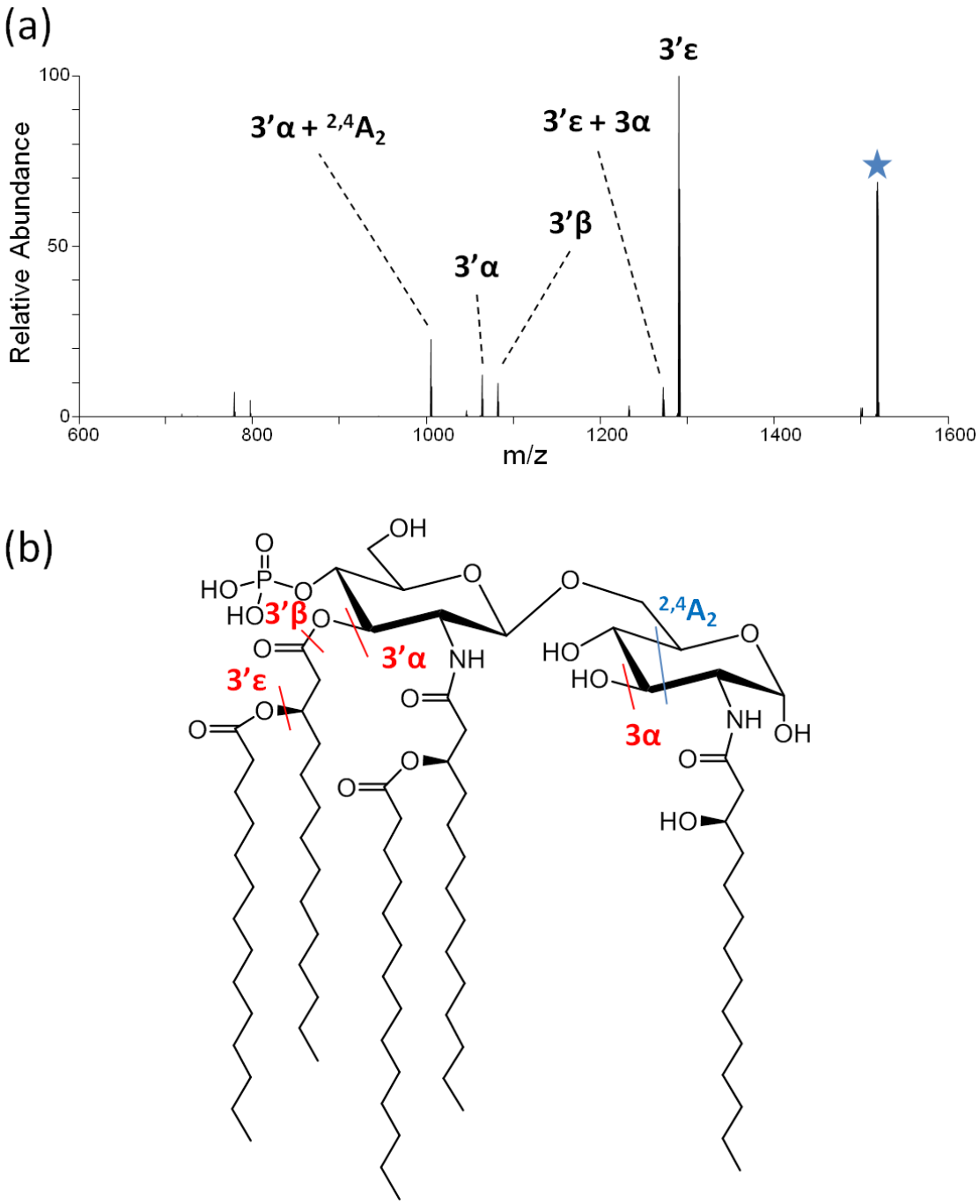

Figure 2.8. MS2 HCD spectra of lAC at NCE=20. The structure of lAC is shown in (b).

The fragmentation behavior of two isomeric lipid A, lAD and lAE, were analyzed in greater detail to evaluate the impact of the position of the phosphate group. For lAD, the phosphate moiety is located on the non-reducing sugar, whereas for lAE the phosphate moiety is located on the reducing sugar. Phosphorylation configurations have been deciphered previously for lipid A molecules from *Yersinia pestis* using MS^n methods [73]. HCD and MS^3 spectra for deprotonated lAD and lAE are shown in **Figure 2.9**. The first stage of HCD results in similar products for the two lipids (dominant cleavage at the 3'α and 2'ε positions), with lAD favoring the 3'α cleavage and lAE favoring the 2'ε cleavage (**Figure 2.9a, b**). Each of these primary products was isolated and subjected to a second stage of HCD, resulting in the MS^3 spectra shown in **Figures 2.9c-f**. Isolation and activation of the dominant 3'α cleavage product for lAD resulted in subsequent cleavage of the O-3 acyl chain (3α or 3β cleavage) or cross ring cleavage of the reducing sugar ($^{0,4}A_2$) (**Figure 2.9c**). In contrast, isolation and activation of the 3'α cleavage product for lAE results in cleavage of the O-3 acyl chain (3α loss) or elimination of the secondary 2' acyl chain (2'ε), the latter not observed for the lAD isomer (**Figure 2.9d**). The striking differences in the MS^3 spectra in **Figure 2.9c, d** highlight the impact of the location of the phosphate group on the consecutive cleavages of acyl chains. Isolation and activation of the 2'ε cleavage products for both lAD and lAE leads to production of two prominent secondary fragment ions via sequential losses of both the 3 and 3' acyl chains (3α and 3'α cleavages in **Figure 2.9e, f**). The order in which these two acyl chains are lost cannot be determined because they have identical masses.

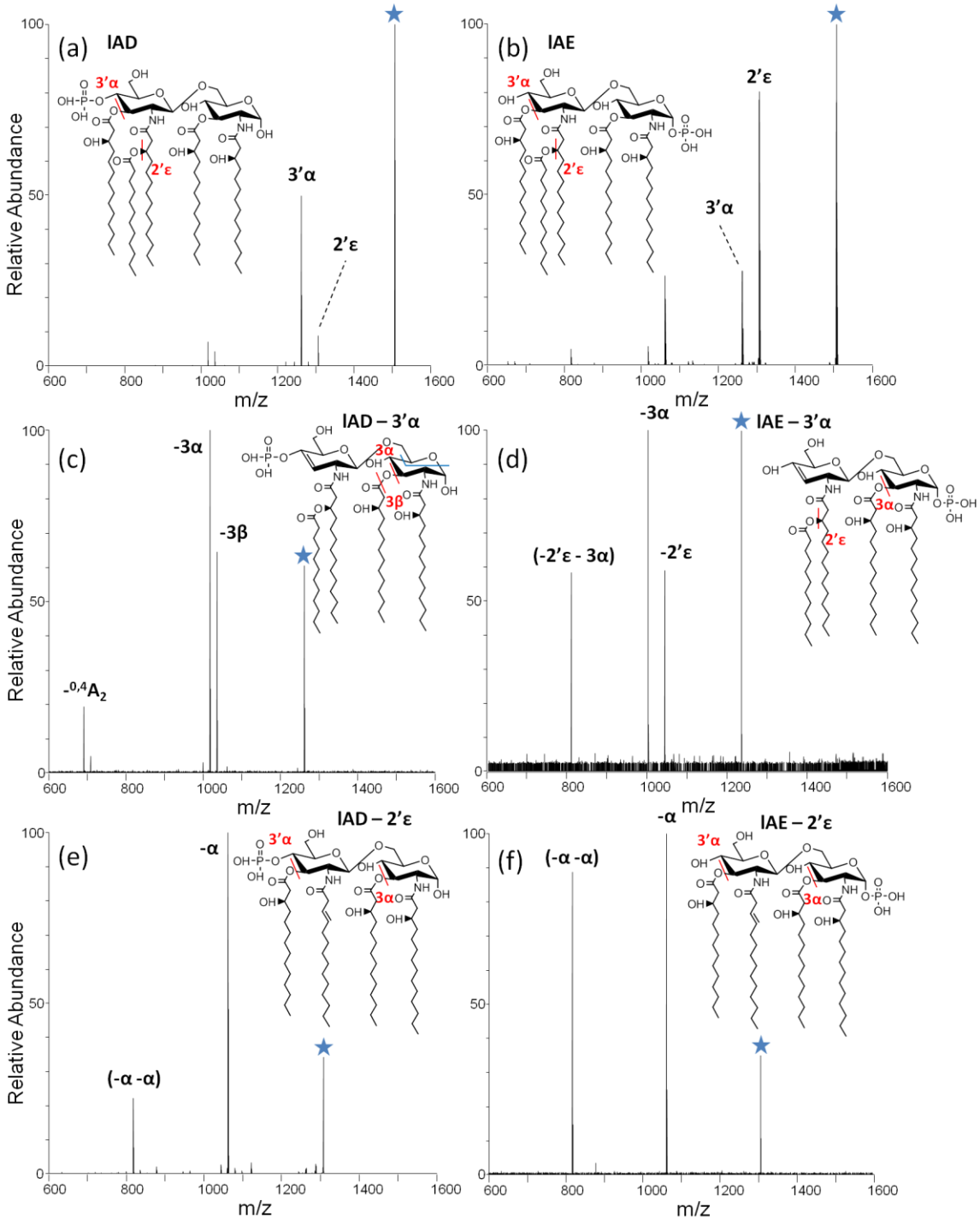

Figure 2.9. HCD spectra of deprotonated (a) lAD and (b) lAE. MS^3 spectra in (c) to (f) reveal the sequential order of 3'α and 2'ε chain cleavage.

Five additional lipid A molecules were analyzed via energy-variable HCD to probe the impact of the number and positions of acyl chains for bis-phosphorylated lipids. Both lAF and lAG have six acyl chains (**Figure 2.10**), the only difference being the location of the secondary acyl chains. lAF has secondary acyl chains located at the 3'- and 2-positions (**Figure 2.10a**), whereas lAG has secondary acyl chains located at the 3'- and 2'-positions (**Figure 2.10b**). The dominant lowest energy fragmentation pathway for both lipids entails cleavage of the secondary acyl chain at the 3' position (3'ε). Sequential fragmentation results in cleavage of two or even three acyl chains at the 3'- and 3-positions. In fact, for these two lipids, eight of the dominant fragmentation pathways are identical. Interestingly, lAF demonstrates a loss of two secondary acyl chains (**Figure 2.10c,** 3'β + 3β + 2ε + PO_3 product), whereas lAG never exhibits the loss of two secondary acyl chains (**Figure 2.10d)**, leading to the conclusion that a secondary acyl chain at the 2-position (2ε) is more labile than one at the 2'-position (2'ε).

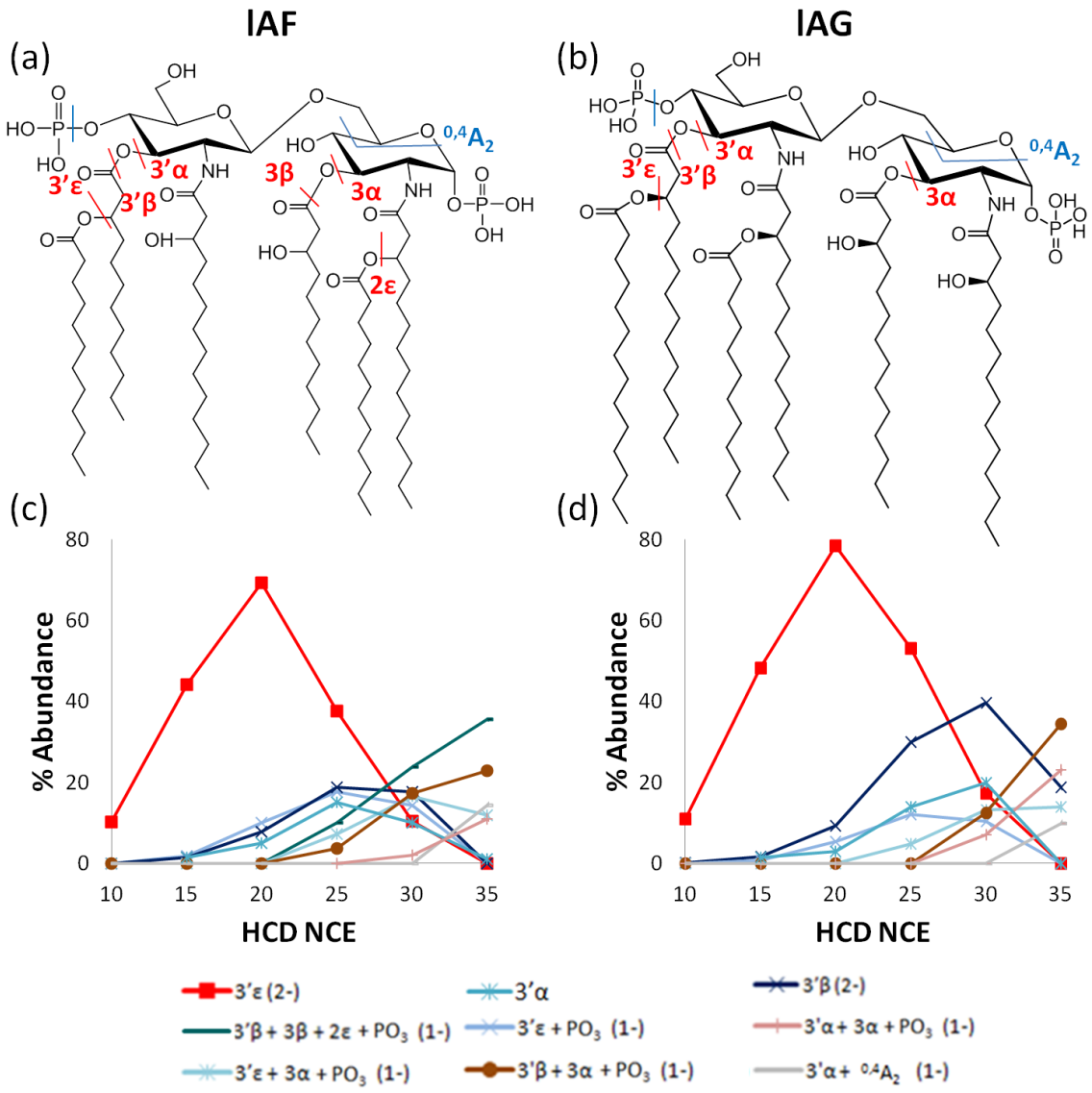

Figure 2.10. Structures of (a) lAF and (b) lAG. The HCD ERMS plots are shown for each doubly deprotonated lipid in (c) and (d), respectively.

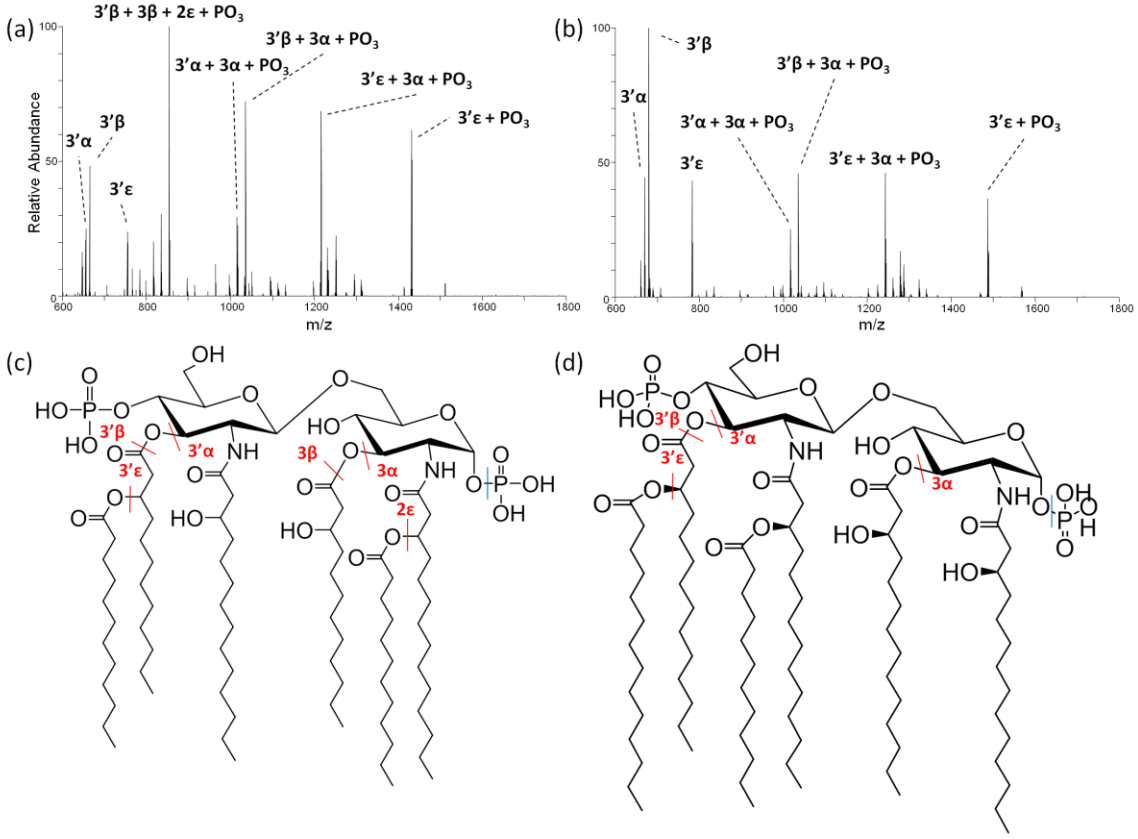

Figure 2.11. MS2 HCD spectra of (a) lAF and (b) lAG at NCE=30 and their structures (c) and (d), respectively.

Three other bisphosphorylated lipid A species were subjected to energy-resolved MS/MS experiments. Of the three species examined, lAH (**Figure 2.12a**) and lAI (**Figure 2.12b**) have a secondary acyl chain at the 3'-position, whereas lAJ (**Figure 2.12c**) has a secondary acyl chain at the 2-position. All three lipids displayed a loss of the secondary acyl chain, whether at the 3'- or 2-position, as the most dominant fragmentation pathway (**Figure 2.12d-f**, 3'ε or 2ε). The HCD spectra and energy-resolved trends for lAH and lAI are nearly identical, an expected outcome for these two analogs that differ only in the length of the secondary acyl chain at the 3' position.

Interestingly, simple loss of the phosphate moiety seems to be a more favored process when the secondary acyl chain is located at the 2-position (in the case of lAJ, **Figure 2.12f**) than when the secondary acyl chain is located at the 3'-position (**Figure 2.12d,e**). Interestingly, the loss of phosphate alone is only prominent for lAJ, the only lipid A with a secondary acyl chain at the 2-position and no other secondary chains. HCD spectra for lAH, lAI, and lAJ can be found in **Figure 2.13**, **Figure 2.14**, and **Figure 2.15**, respectively.

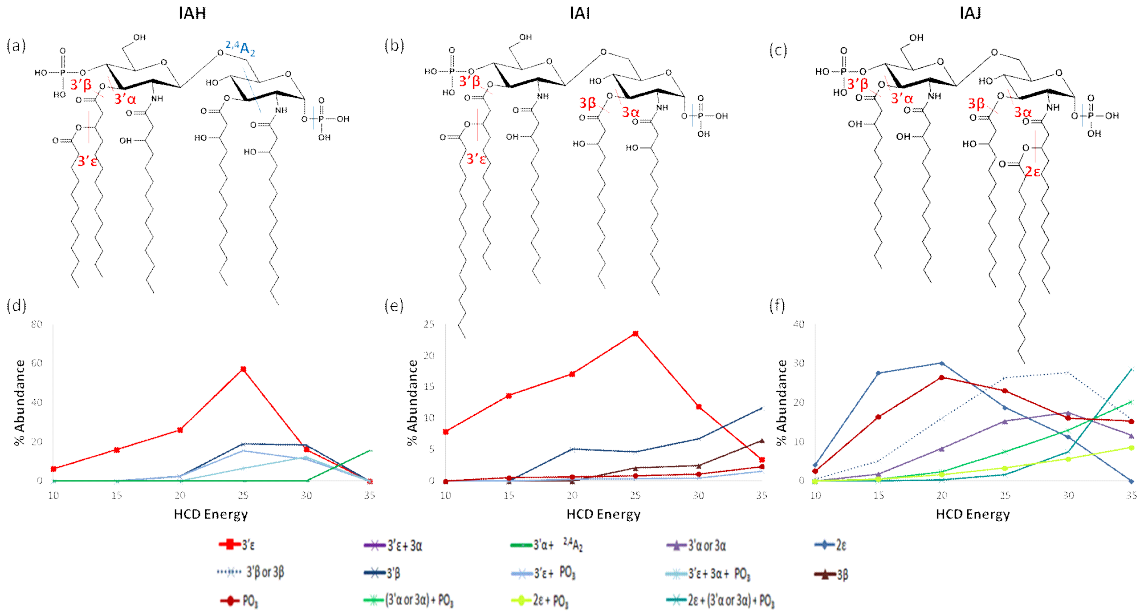

Figure 2.12. lAH, lAI, and lAJ structures with key cleavage sites indicated (a, b, c) and respective HCD ERMS plots (d, e, f) for the deprotonated lipids.

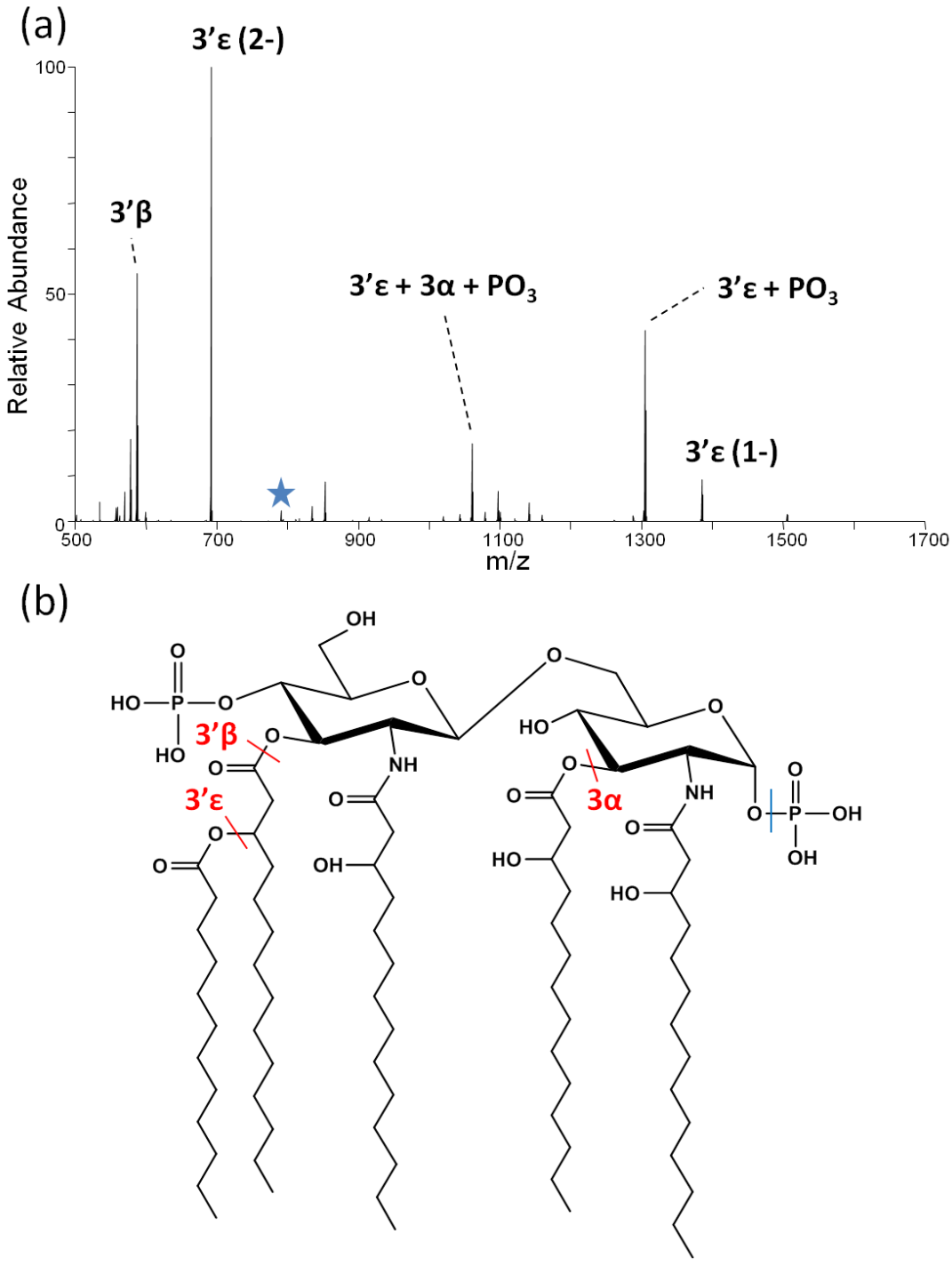

Figure 2.13. lAH MS2 spectra using HCD at NCE=25 (a). The structure of lAH is shown in (b).

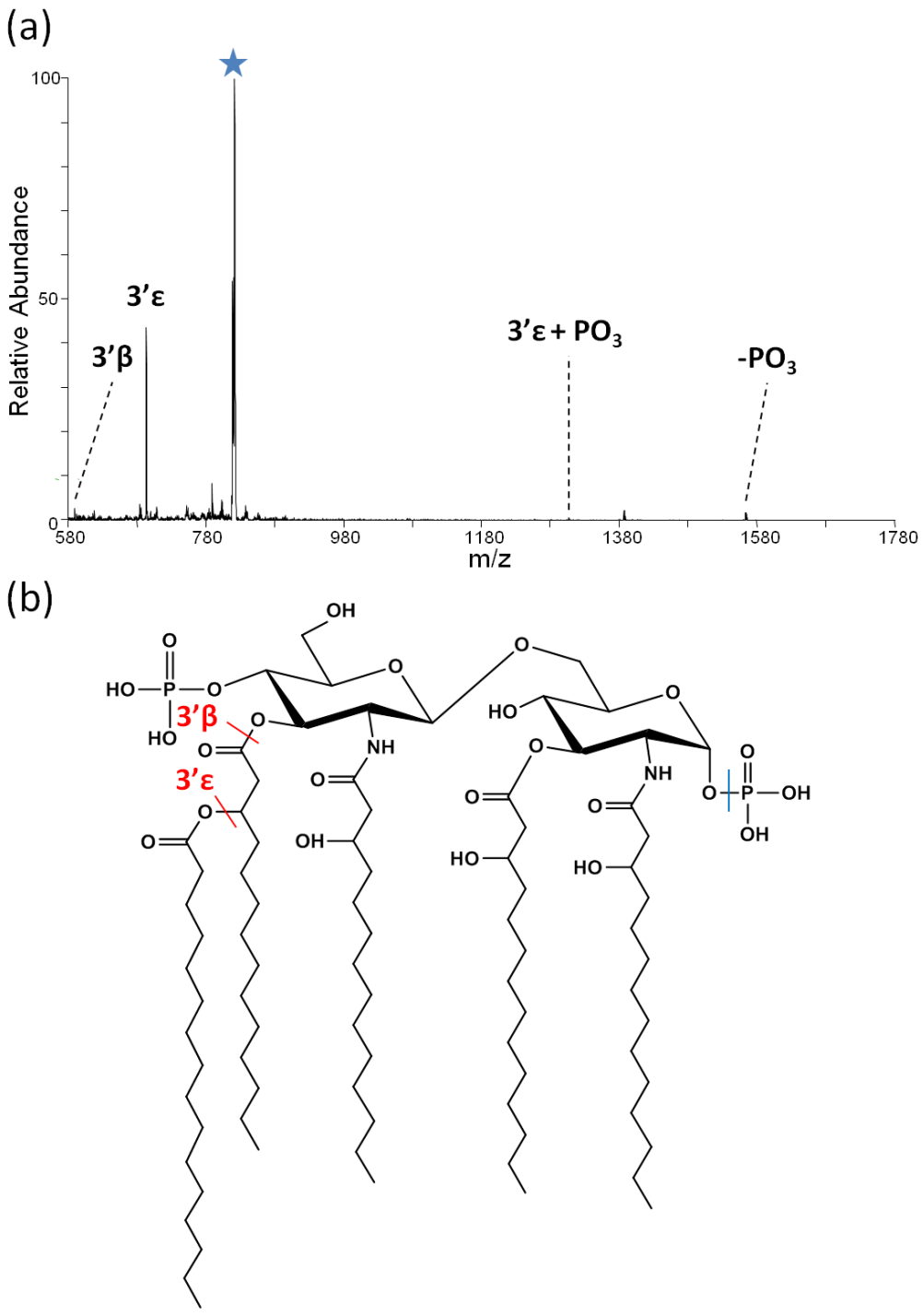

Figure 2.14. lAI MS2 spectra using HCD at NCE=25 (a). The structure of lAI is shown in (b).

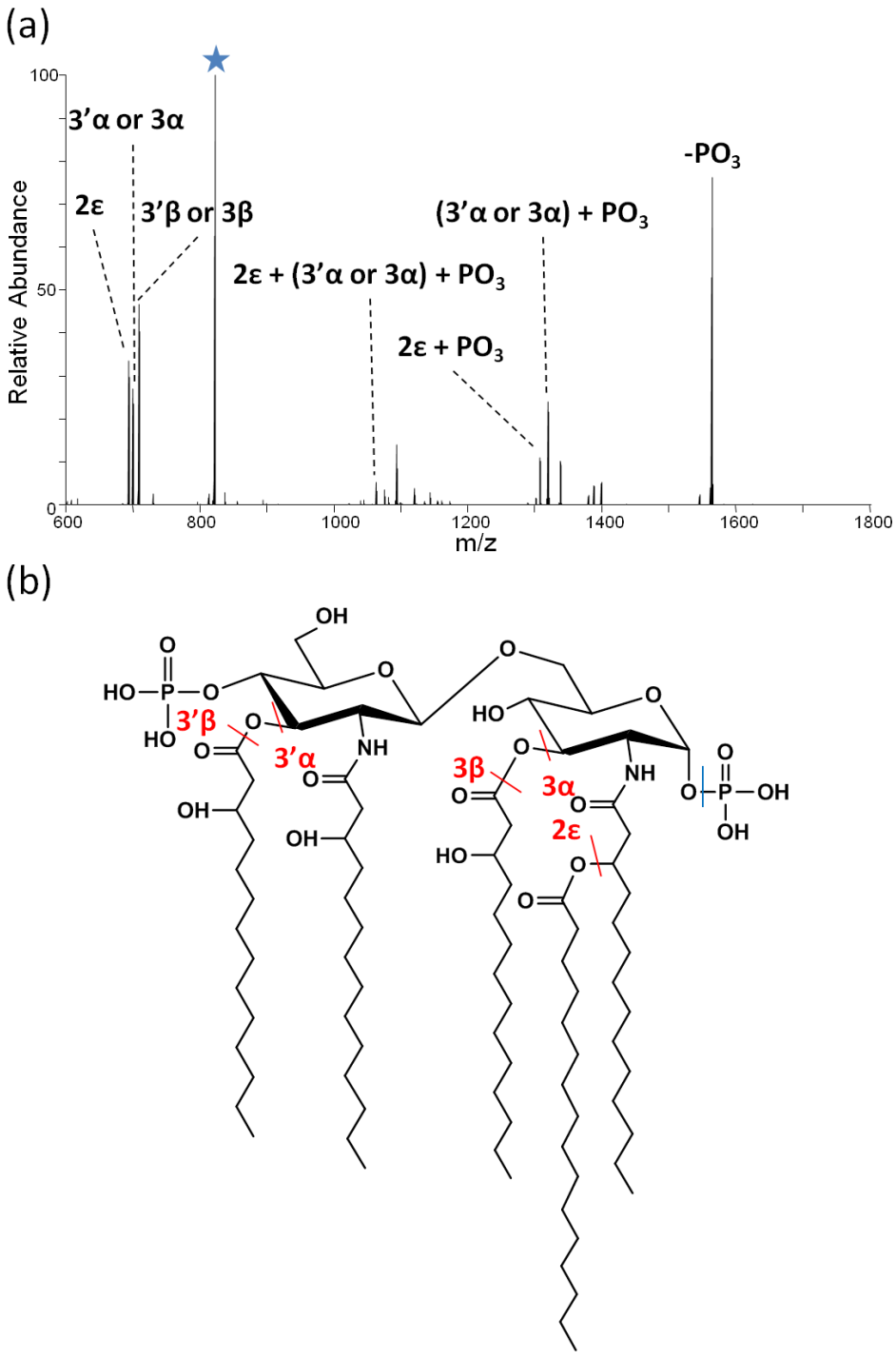

Figure 2.15. lAJ MS2 spectra using HCD at NCE=25 (a). The structure of lAJ is shown in (b).

Several correlations are evident that show the impact of the number of phosphate moieties of lipid A on the fragmentation behavior. In the case of mono-phosphate lAA, the dominant primary and secondary fragment ions observed originated from cleavage of an acyl chain or a cross-ring cleavage occurring (**Figure 2.2**). Analog bis-phosphate lAG shows many of these same characteristics, but competing processes related to phosphate losses are common (**Figure 2.10d**). Phosphate loss from lAA renders the resulting ions non-detectable in the negative mode. Comparison of lAF and lAH shows the influence of the number of secondary chains on the fragmentation patterns. lAF has two secondary acyl chains present, at the 3'- and 2-positions, where lAH has only has a single secondary acyl chain located at the 3'-position. Both molecules favor the 3'ε cleavage, but lAH (**Figure 2.12d**) undergoes phosphate loss more readily than lAF molecule (**Figure 2.10c**). Comparison of lAF to lAJ, lAF demonstrates that the presence of two secondary acyl chain (3'- and 2-positions) facilitates the loss of the phosphate group. The role of a secondary acyl chain located at the 2-position can be evaluated by comparing the fragmentation of lAF to lAH. lAF displays loss of both secondary chains, thus demonstrating the lability of the secondary chains relative to the primary chains.

CONCLUSIONS 2.5

Energy resolved mass spectrometry of lipid A molecules enables detailed characterization of the fragmentation patterns via the genealogical patterns as specific chains are cleaved. HCD yields the most comprehensive information about the combinatorial cleavage of acyl chains and the preferential cleavage of the chains. Cleavage of a 3' secondary chain is most favorable, followed by cleavages of primary

acyl chains at the 3 and 3’ position. For bisphosphorylated lipid A species, loss of a phosphate moiety occurs in conjunction with dominant secondary and primary acyl chain fragmentation. In some instances, cross ring cleavages of the reducing sugar are observed, but the structural features that modulate this pathway have not yet been deciphered.

References

1. Craik, D., Cemazar, M., Daly, N.: The cyclotides and related macrocyclic peptides as scaffolds in drug design. Curr. Opin. Drug Discov. Devel. 9, 251–260 (2006).
2. Craik, D.J.: Seamless Proteins Tie Up Their Loose Ends. Science. 311, 1563–1564 (2006).
3. Chan, P.F., Holmes, D.J., Payne, D.J.: Finding the gems using genomic discovery: antibacterial drug discovery strategies – the successes and the challenges. Drug Discov. Today Ther. Strateg. 1, 519–527 (2004).
4. Diao, L., Meibohm, B.: Pharmacokinetics and Pharmacokinetic–Pharmacodynamic Correlations of Therapeutic Peptides. Clin. Pharmacokinet. 52, 855–868 (2013).
5. Horton, D.A., Bourne, G.T., Smythe, M.L.: Exploring privileged structures: The combinatorial synthesis of cyclic peptides. Mol. Divers. 5, 289–304 (2000).
6. Rose, L., Jenkins, A.T.A.: The effect of the ionophore valinomycin on biomimetic solid supported lipid DPPTE/EPC membranes. Bioelectrochemistry. 70, 387–393 (2007).
7. Dathe, M., Nikolenko, H., Klose, J., Bienert, M.: Cyclization Increases the Antimicrobial Activity and Selectivity of Arginine- and Tryptophan-Containing Hexapeptides†. Biochemistry (Mosc.). 43, 9140–9150 (2004).
8. Eckart, K.: Mass spectrometry of cyclic peptides. Mass Spectrom. Rev. 13, 23–55 (1994).
9. Johnson, A.R., Carlson, E.E.: Collision-Induced Dissociation Mass Spectrometry: A Powerful Tool for Natural Product Structure Elucidation. Anal. Chem. (2015).
10. Stawikowski, M., Cudic, P.: Depsipeptide Synthesis. In: Fields, G.B. (ed.) Peptide Characterization and Application Protocols. pp. 321–339. Humana Press (2007).
11. Fernandez-Lopez, S., Kim, H.-S., Choi, E.C., Delgado, M., Granja, J.R., Khasanov, A., Kraehenbuehl, K., Long, G., Weinberger, D.A., Wilcoxen, K.M., Ghadiri, M.R.: Antibacterial agents based on the cyclic d,l-α-peptide architecture. Nature. 412, 452–455 (2001).
12. Visconti, A., Blais, L.A., ApSimon, J.W., Greenhalgh, R., Miller, J.D.: Production of enniatins by Fusarium acuminatum and Fusarium compactum in liquid culture: isolation and characterization of three new enniatins, B2, B3, and B4. J. Agric. Food Chem. 40, 1076–1082 (1992).
13. Millward, S.W., Fiacco, S., Austin, R.J., Roberts, R.W.: Design of Cyclic Peptides That Bind Protein Surfaces with Antibody-Like Affinity. ACS Chem. Biol. 2, 625–634 (2007).
14. Kim, Y.-W., Grossmann, T.N., Verdine, G.L.: Synthesis of all-hydrocarbon stapled α-helical peptides by ring-closing olefin metathesis. Nat. Protoc. 6, 761–771 (2011).
15. Kawamoto, S.A., Coleska, A., Ran, X., Yi, H., Yang, C.-Y., Wang, S.: Design of Triazole-Stapled BCL9 α-Helical Peptides to Target the β-Catenin/B-Cell CLL/lymphoma 9 (BCL9) Protein–Protein Interaction. J. Med. Chem. 55, 1137–1146 (2012).

16. Agnew, H.D., Rohde, R.D., Millward, S.W., Nag, A., Yeo, W.-S., Hein, J.E., Pitram, S.M., Tariq, A.A., Burns, V.M., Krom, R.J., Fokin, V.V., Sharpless, K.B., Heath, J.R.: Iterative In Situ Click Chemistry Creates Antibody-like Protein-Capture Agents. Angew. Chem. Int. Ed. 48, 4944–4948 (2009).
17. Millward, S.W., Agnew, H.D., Lai, B., Lee, S.S., Lim, J., Nag, A., Pitram, S., Rohde, R., Heath, J.R.: In situ click chemistry: from small molecule discovery to synthetic antibodies. Integr. Biol. 5, 87–95 (2012).
18. Millward, S.W., Henning, R.K., Kwong, G.A., Pitram, S., Agnew, H.D., Deyle, K.M., Nag, A., Hein, J., Lee, S.S., Lim, J., Pfeilsticker, J.A., Sharpless, K.B., Heath, J.R.: Iterative in Situ Click Chemistry Assembles a Branched Capture Agent and Allosteric Inhibitor for Akt1. J. Am. Chem. Soc. 133, 18280–18288 (2011).
19. Pressman, B.C.: Biological Applications of Ionophores. Annu. Rev. Biochem. 45, 501–530 (1976).
20. Duax, W.L., Griffin, J.F., Langs, D.A., Smith, G.D., Grochulski, P., Pletnev, V., Ivanov, V.: Molecular structure and mechanisms of action of cyclic and linear ion transport antibiotics. Pept. Sci. 40, 141–155 (1996).
21. Quimbar, P., Malik, U., Sommerhoff, C.P., Kaas, Q., Chan, L.Y., Huang, Y.-H., Grundhuber, M., Dunse, K., Craik, D.J., Anderson, M.A., Daly, N.L.: High-affinity Cyclic Peptide Matriptase Inhibitors. J. Biol. Chem. 288, 13885–13896 (2013).
22. Pavlaskova, K., Nedved, J., Kuzma, M., Zabka, M., Sulc, M., Sklenar, J., Novak, P., Benada, O., Kofronova, O., Hajduch, M., Derrick, P.J., Lemr, K., Jegorov, A., Havlicek, V.: Characterization of Pseudacyclins A−E, a Suite of Cyclic Peptides Produced by Pseudallescheria boydii. J. Nat. Prod. 73, 1027–1032 (2010).
23. Ngoka, L.C.M., Gross, M.L.: Multistep tandem mass spectrometry for Sequencing Cyclic Peptides in an Ion-Trap Mass Spectrometer. J. Am. Soc. Mass Spectrom. 10, 732–746 (1999).
24. Ciccimaro, E., Ranasinghe, A., D'Arienzo, C., Xu, C., Onorato, J., Drexler, D.M., Josephs, J.L., Poss, M., Olah, T.: Strategy to Improve the Quantitative LC-MS Analysis of Molecular Ions Resistant to Gas-Phase Collision Induced Dissociation: Application to Disulfide-Rich Cyclic Peptides. Anal. Chem. 86, 11523–11527 (2014).
25. Siegel, M.M., Huang, J., Lin, B., Tsao, R., Edmonds, C.G.: Structures of bacitracin A and isolated congeners: Sequencing of cyclic peptides with blocked linear side chains by electrospray ionization mass spectrometry. Biol. Mass Spectrom. 23, 186–204 (1994).
26. Niedermeyer, T.H.J., Strohalm, M.: mMass as a Software Tool for the Annotation of Cyclic Peptide Tandem Mass Spectra. PLoS ONE. 7, e44913 (2012).
27. Mohimani, H., Yang, Y.-L., Liu, W.-T., Hsieh, P.-W., Dorrestein, P.C., Pevzner, P.A.: Sequencing cyclic peptides by multistage mass spectrometry. PROTEOMICS. 11, 3642–3650 (2011).
28. Cooper, H.J., Hudgins, R.R., Marshall, A.G.: Electron capture dissociation Fourier transform ion cyclotron resonance mass spectrometry of cyclodepsipeptides, branched peptides, and ε-peptides. Int. J. Mass Spectrom. 234, 23–35 (2004).

29. Williams, S.M., Brodbelt, J.S.: MSn characterization of protonated cyclic peptides and metal complexes. J. Am. Soc. Mass Spectrom. 15, 1039–1054 (2004).
30. Kimbrell, J.B., Hite, J.R., Skala, K.N., Crittenden, C.M., Richardson, C.N., Mruthinti, S.S., Fujita, M., Khan, F.A.: Direct binding of halide ions by valinomycin. Supramol. Chem. 23, 782–789 (2011).
31. Schwartz, B.L., Bursey, M.M.: Some proline substituent effects in the tandem mass spectrum of protonated pentaalanine. Biol. Mass Spectrom. 21, 92–96 (1992).
32. Raulfs, M.D.M., Breci, L., Bernier, M., Hamdy, O.M., Janiga, A., Wysocki, V., Poutsma, J.C.: Investigations of the Mechanism of the "Proline Effect" in Tandem Mass Spectrometry Experiments: The "Pipecolic Acid Effect." J. Am. Soc. Mass Spectrom. 25, 1705–1715 (2014).
33. Leitner, A., Lindner, W.: Chemistry meets proteomics: The use of chemical tagging reactions for MS-based proteomics. PROTEOMICS. 6, 5418–5434 (2006).
34. García-Murria, M.J., Valero, M.L., Sánchez del Pino, M.M.: Simple chemical tools to expand the range of proteomics applications. J. Proteomics. 74, 137–150 (2011).
35. Liu, Z., Julian, R.R.: Deciphering the Peptide Iodination Code: Influence on Subsequent Gas-Phase Radical Generation with Photodissociation ESI-MS. J. Am. Soc. Mass Spectrom. 20, 965–971 (2009).
36. Sun, Q., Yin, S., Loo, J.A., Julian, R.R.: Radical Directed Dissociation for Facile Identification of Iodotyrosine Residues Using Electrospray Ionization Mass Spectrometry. Anal. Chem. 82, 3826–3833 (2010).
37. Gardner, M.W., Brodbelt, J.S.: Ultraviolet Photodissociation Mass Spectrometry of Bis-aryl Hydrazone Conjugated Peptides. Anal. Chem. 81, 4864–4872 (2009).
38. Vasicek, L., O'Brien, J.P., Browning, K.S., Tao, Z., Liu, H.-W., Brodbelt, J.S.: Mapping Protein Surface Accessibility via an Electron Transfer Dissociation Selectively Cleavable Hydrazone Probe. Mol. Cell. Proteomics. 11, O111.015826 (2012).
39. Bishop, A., Brodbelt, J.S.: Selective cleavage upon ETD of peptides containing disulfide or nitrogen–nitrogen bonds. Int. J. Mass Spectrom. 378, 127–133 (2015).
40. McGee, W.M., McLuckey, S.A.: The ornithine effect in peptide cation dissociation. J. Mass Spectrom. 48, 856–861 (2013).
41. Prentice, B.M., McGee, W.M., Stutzman, J.R., McLuckey, S.A.: Strategies for the Gas Phase Modification of Cationized Arginine via Ion/ion Reactions. Int. J. Mass Spectrom. 354–355, (2013).
42. Schroeder, O.E., Andriole, E.J., Carver, K.L., Colyer, K.E., Poutsma, J.C.: Proton Affinity of Lysine Homologues from the Extended Kinetic Method. J. Phys. Chem. A. 108, 326–332 (2004).
43. Bleiholder, C., Osburn, S., Williams, T.D., Suhai, S., Van Stipdonk, M., Harrison, A.G., Paizs, B.: Sequence-Scrambling Fragmentation Pathways of Protonated Peptides. J. Am. Chem. Soc. 130, 17774–17789 (2008).
44. Molesworth, S., Osburn, S., Van Stipdonk, M.: Influence of Amino Acid Side Chains on Apparent Selective Opening of Cyclic b5 Ions. J. Am. Soc. Mass Spectrom. 21, 1028–1036 (2010).

45. Atik, A.E., Gorgulu, G., Yalcin, T.: The role of lysine ε-amine group on the macrocyclization of b ions. Int. J. Mass Spectrom. 316–318, 84–90 (2012).
46. Vasicek, L.A., Ledvina, A.R., Shaw, J., Griep-Raming, J., Westphall, M.S., Coon, J.J., Brodbelt, J.S.: Implementing photodissociation in an Orbitrap mass spectrometer. J. Am. Soc. Mass Spectrom. 22, 1105–1108 (2011).
47. Shaw, J.B., Li, W., Holden, D.D., Zhang, Y., Griep-Raming, J., Fellers, R.T., Early, B.P., Thomas, P.M., Kelleher, N.L., Brodbelt, J.S.: Complete Protein Characterization Using Top-Down Mass Spectrometry and Ultraviolet Photodissociation. J. Am. Chem. Soc. 135, 12646–12651 (2013).
48. Kavan, D., Kuzma, M., Lemr, K., Schug, K.A., Havlicek, V.: CYCLONE—A Utility for De Novo Sequencing of Microbial Cyclic Peptides. J. Am. Soc. Mass Spectrom. 24, 1177–1184 (2013).
49. Novák, J., Lemr, K., Schug, K.A., Havlíček, V.: CycloBranch: De Novo Sequencing of Nonribosomal Peptides from Accurate Product Ion Mass Spectra. J. Am. Soc. Mass Spectrom. 1–7 (2015).
50. Owens, M.: Embedding an SQL Database with SQLite. Linux J. 2003, 2– (2003).
51. Luckett, S., Garcia, R.S., Barker, J.J., Konarev, A.V., Shewry, P.R., Clarke, A.R., Brady, R.L.: High-resolution structure of a potent, cyclic proteinase inhibitor from sunflower seeds1. J. Mol. Biol. 290, 525–533 (1999).
52. Colgrave, M.L., Korsinczky, M.J.L., Clark, R.J., Foley, F., Craik, D.J.: Sunflower trypsin inhibitor-1, proteolytic studies on a trypsin inhibitor peptide and its analogs. Pept. Sci. 94, 665–672 (2010).
53. Kaye, K.S., Pogue, J.M.: Infections Caused by Resistant Gram-Negative Bacteria: Epidemiology and Management. Pharmacother. J. Hum. Pharmacol. Drug Ther. 35, 949–962 (2015).
54. Bouchillon, S.K., Badal, R.E., Hoban, D.J., Hawser, S.P.: Antimicrobial Susceptibility of Inpatient Urinary Tract Isolates of Gram-Negative Bacilli in the United States: Results from the Study for Monitoring Antimicrobial Resistance Trends (SMART) Program: 2009−2011. Clin. Ther. 35, 872–877 (2013).
55. Bush, K.: Investigational Agents for the Treatment of Gram-Negative Bacterial Infections: A Reality Check. ACS Infect. Dis. 1, 509–511 (2015).
56. Kollef, M.H., Golan, Y., Micek, S.T., Shorr, A.F., Restrepo, M.I.: Appraising Contemporary Strategies to Combat Multidrug Resistant Gram-Negative Bacterial Infections–Proceedings and Data From the Gram-Negative Resistance Summit. Clin. Infect. Dis. 53, S33–S55 (2011).
57. Whitfield, C., Trent, M.S.: Biosynthesis and export of bacterial lipopolysaccharides. Annu. Rev. Biochem. 83, 99–128 (2014).
58. Needham, B.D., Trent, M.S.: Fortifying the barrier: the impact of lipid A remodelling on bacterial pathogenesis. Nat. Rev. Microbiol. 11, 467–481 (2013).
59. Alexander, C., Rietschel, E.T.: Bacterial lipopolysaccharides and innate immunity. J. Endotoxin Res. 7, 167–202 (2001).
60. Caroff, M., Karibian, D.: Structure of bacterial lipopolysaccharides. Carbohydr. Res. 338, 2431–2447 (2003).

61. Takayama, K., Qureshi, N., Ribi, E., Cantrell, J.L.: Separation and characterization of toxic and nontoxic forms of lipid A. Rev. Infect. Dis. 6, 439–443 (1984).
62. Kabanov, D.S., Prokhorenko, I.R.: Structural analysis of lipopolysaccharides from Gram-negative bacteria. Biochem. Mosc. 75, 383–404 (2010).
63. Raetz, C.R.H., Reynolds, C.M., Trent, M.S., Bishop, R.E.: Lipid A modification systems in gram-negative bacteria. Annu. Rev. Biochem. 76, 295–329 (2007).
64. Rietschel, E.T., Wollenweber, H.W., Zähringer, U., Lüderitz, O.: Lipid A, the lipid component of bacterial lipopolysaccharides: relation of chemical structure to biological activity. Klin. Wochenschr. 60, 705–709 (1982).
65. Corsaro, M.M., Piaz, F.D., Lanzetta, R., Parrilli, M.: Lipid A structure of Pseudoalteromonas haloplanktis TAC 125: use of electrospray ionization tandem mass spectrometry for the determination of fatty acid distribution. J. Mass Spectrom. JMS. 37, 481–488 (2002).
66. Bedoux, G., Vallée-Réhel, K., Kooistra, O., Zähringer, U., Haras, D.: Lipid A components from Pseudomonas aeruginosa PAO1 (serotype O5) and mutant strains investigated by electrospray ionization ion-trap mass spectrometry. J. Mass Spectrom. JMS. 39, 505–513 (2004).
67. Lee, C.-S., Kim, Y.-G., Joo, H.-S., Kim, B.-G.: Structural analysis of lipid A from Escherichia coli O157:H7:K- using thin-layer chromatography and ion-trap mass spectrometry. J. Mass Spectrom. JMS. 39, 514–525 (2004).
68. Sforza, S., Silipo, A., Molinaro, A., Marchelli, R., Parrilli, M., Lanzetta, R.: Determination of fatty acid positions in native lipid A by positive and negative electrospray ionization mass spectrometry. J. Mass Spectrom. JMS. 39, 378–383 (2004).
69. El-Aneed, A., Banoub, J.: Elucidation of the molecular structure of lipid A isolated from both a rough mutant and a wild strain of Aeromonas salmonicida lipopolysaccharides using electrospray ionization quadrupole time-of-flight tandem mass spectrometry. Rapid Commun. Mass Spectrom. RCM. 19, 1683–1695 (2005).
70. Shaffer, S.A., Harvey, M.D., Goodlett, D.R., Ernst, R.K.: Structural heterogeneity and environmentally regulated remodeling of Francisella tularensis subspecies novicida lipid a characterized by tandem mass spectrometry. J. Am. Soc. Mass Spectrom. 18, 1080–1092 (2007).
71. Schilling, B., McLendon, M.K., Phillips, N.J., Apicella, M.A., Gibson, B.W.: Characterization of lipid A acylation patterns in Francisella tularensis, Francisella novicida, and Francisella philomiragia using multiple-stage mass spectrometry and matrix-assisted laser desorption/ionization on an intermediate vacuum source linear ion trap. Anal. Chem. 79, 1034–1042 (2007).
72. Silipo, A., De Castro, C., Lanzetta, R., Molinaro, A., Parrilli, M., Vago, G., Sturiale, L., Messina, A., Garozzo, D.: Structural characterizations of lipids A by MS/MS of doubly charged ions on a hybrid linear ion trap/orbitrap mass spectrometer. J. Mass Spectrom. JMS. 43, 478–484 (2008).
73. Jones, J.W., Cohen, I.E., Tureĉek, F., Goodlett, D.R., Ernst, R.K.: Comprehensive structure characterization of lipid a extracted from Yersinia pestis for determination

of its phosphorylation configuration. J. Am. Soc. Mass Spectrom. 21, 785–799 (2010).
74. Brodbelt, J.S.: Photodissociation mass spectrometry: new tools for characterization of biological molecules. Chem. Soc. Rev. 43, 2757–2783 (2014).
75. Reilly, J.P.: Ultraviolet photofragmentation of biomolecular ions. Mass Spectrom. Rev. 28, 425–447 (2009).
76. Ly, T., Julian, R.R.: Ultraviolet Photodissociation: Developments towards Applications for Mass-Spectrometry-Based Proteomics. Angew. Chem. Int. Ed. 48, 7130–7137 (2009).
77. Madsen, J.A., Boutz, D.R., Brodbelt, J.S.: Ultrafast Ultraviolet Photodissociation at 193 nm and its Applicability to Proteomic Workflows. J. Proteome Res. 9, 4205–4214 (2010).
78. Madsen, J.A., Cullen, T.W., Trent, M.S., Brodbelt, J.S.: IR and UV Photodissociation as Analytical Tools for Characterizing Lipid A Structures. Anal. Chem. 83, 5107–5113 (2011).
79. O'Brien, J.P., Needham, B.D., Henderson, J.C., Nowicki, E.M., Trent, M.S., Brodbelt, J.S.: 193 nm Ultraviolet Photodissociation Mass Spectrometry for the Structural Elucidation of Lipid A Compounds in Complex Mixtures. Anal. Chem. 86, 2138–2145 (2014).
80. Hankins, J.V., Madsen, J.A., Giles, D.K., Childers, B.M., Klose, K.E., Brodbelt, J.S., Trent, M.S.: Elucidation of a novel Vibrio cholerae lipid A secondary hydroxy-acyltransferase and its role in innate immune recognition. Mol. Microbiol. 81, 1313–1329 (2011).
81. Hankins, J.V., Madsen, J.A., Giles, D.K., Brodbelt, J.S., Trent, M.S.: Amino acid addition to Vibrio cholerae LPS establishes a link between surface remodeling in gram-positive and gram-negative bacteria. Proc. Natl. Acad. Sci. U. S. A. 109, 8722–8727 (2012).
82. Hankins, J.V., Madsen, J.A., Needham, B.D., Brodbelt, J.S., Trent, M.S.: The outer membrane of Gram-negative bacteria: lipid A isolation and characterization. Methods Mol. Biol. Clifton NJ. 966, 239–258 (2013).
83. Cullen, T.W., O'Brien, J.P., Hendrixson, D.R., Giles, D.K., Hobb, R.I., Thompson, S.A., Brodbelt, J.S., Trent, M.S.: EptC of Campylobacter jejuni Mediates Phenotypes Involved in Host Interactions and Virulence. Infect. Immun. 81, 430–440 (2013).
84. Rubin, E.J., O'Brien, J.P., Ivanov, P.L., Brodbelt, J.S., Trent, M.S.: Identification of a broad family of lipid A late acyltransferases with non-canonical substrate specificity. Mol. Microbiol. 91, 887–899 (2014).
85. O'Brien, J.P., Needham, B.D., Brown, D.B., Trent, M.S., Brodbelt, J.S.: Top-Down Strategies for the Structural Elucidation of Intact Gram-negative Bacterial Endotoxins. Chem. Sci. R. Soc. Chem. 2010. 5, 4291–4301 (2014).
86. Ting, Y.S., Shaffer, S.A., Jones, J.W., Ng, W.V., Ernst, R.K., Goodlett, D.R.: Automated Lipid A Structure Assignment from Hierarchical Tandem Mass Spectrometry Data. J. Am. Soc. Mass Spectrom. 22, 856–866 (2011).

87. Morrison, L.J., Parker, W.R., Holden, D.D., Henderson, J.C., Boll, J.M., Trent, M.S., Brodbelt, J.S.: UVliPiD: A UVPD-Based Hierarchical Approach for De Novo Characterization of Lipid A Structures. Anal. Chem. 88, 1812–1820 (2016).
88. Kolli, V., Dodds, E.D.: Energy-resolved collision-induced dissociation pathways of model N-linked glycopeptides: implications for capturing glycan connectivity and peptide sequence in a single experiment. Analyst. 139, 2144–2153 (2014).
89. Kurimoto, A., Daikoku, S., Mutsuga, S., Kanie, O.: Analysis of Energy-Resolved Mass Spectra at MSn in a Pursuit To Characterize Structural Isomers of Oligosaccharides. Anal. Chem. 78, 3461–3466 (2006).
90. Nowicki, E.M., O'Brien, J.P., Brodbelt, J.S., Trent, M.S.: Extracellular zinc induces phosphoethanolamine addition to Pseudomonas aeruginosa lipid A via the ColRS two-component system. Mol. Microbiol. 97, 166–178 (2015).
91. Needham, B.D., Carroll, S.M., Giles, D.K., Georgiou, G., Whiteley, M., Trent, M.S.: Modulating the innate immune response by combinatorial engineering of endotoxin. Proc. Natl. Acad. Sci. 110, 1464–1469 (2013).
92. Klein, D.R., Holden, D.D., Brodbelt, J.S.: Shotgun Analysis of Rough-Type Lipopolysaccharides Using Ultraviolet Photodissociation Mass Spectrometry. Anal. Chem. 88, 1044–1051 (2016).
93. Domon, B., Costello, C.E.: A systematic nomenclature for carbohydrate fragmentations in FAB-MS/MS spectra of glycoconjugates. Glycoconj. J. 5, 397–409 (1988).
94. Gabelica, V., Tabarin, T., Antoine, R., Rosu, F., Compagnon, I., Broyer, M., De Pauw, E., Dugourd, P.: Electron Photodetachment Dissociation of DNA Polyanions in a Quadrupole Ion Trap Mass Spectrometer. Anal. Chem. 78, 6564–6572 (2006).